arXiv:hep-ex/0701051v1 28 Jan 2007

Measurement of the Inclusive Jet Cross Section using the k_{T} algorithm in $p\overline{p}$ Collisions at $\sqrt{s} = 1.96$ TeV with the CDF II Detector

A. Abulencia,[24] J. Adelman,[13] T. Affolder,[10] T. Akimoto,[56] M.G. Albrow,[17] D. Ambrose,[17] S. Amerio,[44] D. Amidei,[35] A. Anastassov,[53] K. Anikeev,[17] A. Annovi,[19] J. Antos,[14] M. Aoki,[56] G. Apollinari,[17] J.-F. Arguin,[34] T. Arisawa,[58] A. Artikov,[15] W. Ashmanskas,[17] A. Attal,[8] F. Azfar,[43] P. Azzi-Bacchetta,[44] P. Azzurri,[47] N. Bacchetta,[44] W. Badgett,[17] A. Barbaro-Galtieri,[29] V.E. Barnes,[49] B.A. Barnett,[25] S. Baroiant,[7] V. Bartsch,[31] G. Bauer,[33] F. Bedeschi,[47] S. Behari,[25] S. Belforte,[55] G. Bellettini,[47] J. Bellinger,[60] A. Belloni,[33] D. Benjamin,[16] A. Beretvas,[17] J. Beringer,[29] T. Berry,[30] A. Bhatti,[51] M. Binkley,[17] D. Bisello,[44] R.E. Blair,[2] C. Blocker,[6] B. Blumenfeld,[25] A. Bocci,[16] A. Bodek,[50] V. Boisvert,[50] G. Bolla,[49] A. Bolshov,[33] D. Bortoletto,[49] J. Boudreau,[48] A. Boveia,[10] B. Brau,[10] L. Brigliadori,[5] C. Bromberg,[36] E. Brubaker,[13] J. Budagov,[15] H.S. Budd,[50] S. Budd,[24] S. Budroni,[47] K. Burkett,[17] G. Busetto,[44] P. Bussey,[21] K. L. Byrum,[2] S. Cabrera^{o},[16] M. Campanelli,[20] M. Campbell,[35] F. Canelli,[17] A. Canepa,[49] S. Carillo^{i},[18] D. Carlsmith,[60] R. Carosi,[47] S. Carron,[34] M. Casarsa,[55] A. Castro,[5] P. Catastini,[47] D. Cauz,[55] M. Cavalli-Sforza,[3] A. Cerri,[29] L. Cerrito^{m},[43] S.H. Chang,[28] Y.C. Chen,[1] M. Chertok,[7] G. Chiarelli,[47] G. Chlachidze,[15] F. Chlebana,[17] I. Cho,[28] K. Cho,[28] D. Chokheli,[15] J.P. Chou,[22] G. Choudalakis,[33] S.H. Chuang,[60] K. Chung,[12] W.H. Chung,[60] Y.S. Chung,[50] M. Ciljak,[47] C.I. Ciobanu,[24] M.A. Ciocci,[47] A. Clark,[20] D. Clark,[6] M. Coca,[16] G. Compostella,[44] M.E. Convery,[51] J. Conway,[7] B. Cooper,[36] K. Copic,[35] M. Cordelli,[19] G. Cortiana,[44] F. Crescioli,[47] C. Cuenca Almenar^{o},[7] J. Cuevas^{l},[11] R. Culbertson,[17] J.C. Cully,[35] D. Cyr,[60] S. DaRonco,[44] M. Datta,[17] S. D'Auria,[21] T. Davies,[21] M. D'Onofrio,[3] D. Dagenhart,[6] P. de Barbaro,[50] S. De Cecco,[52] A. Deisher,[29] G. De Lentdecker^{c},[50] M. Dell'Orso,[47] F. Delli Paoli,[44] L. Demortier,[51] J. Deng,[16] M. Deninno,[5] D. De Pedis,[52] P.F. Derwent,[17] G.P. Di Giovanni,[45] C. Dionisi,[52] B. Di Ruzza,[55] J.R. Dittmann,[4] P. DiTuro,[53] C. Dörr,[26] S. Donati,[47] M. Donega,[20] P. Dong,[8] J. Donini,[44] T. Dorigo,[44] S. Dube,[53] J. Efron,[40] R. Erbacher,[7] D. Errede,[24] S. Errede,[24] R. Eusebi,[17] H.C. Fang,[29] S. Farrington,[30] I. Fedorko,[47] W.T. Fedorko,[13] R.G. Feild,[61] M. Feindt,[26] J.P. Fernandez,[32] R. Field,[18] G. Flanagan,[49] A. Foland,[22] S. Forrester,[7] G.W. Foster,[17] M. Franklin,[22] J.C. Freeman,[29] I. Furic,[13] M. Gallinaro,[51] J. Galyardt,[12] J.E. Garcia,[47] F. Garberson,[10] A.F. Garfinkel,[49] C. Gay,[61] H. Gerberich,[24] D. Gerdes,[35] S. Giagu,[52] P. Giannetti,[47] A. Gibson,[29] K. Gibson,[48] J.L. Gimmell,[50] C. Ginsburg,[17] N. Giokaris^{a},[15] M. Giordani,[55] P. Giromini,[19] M. Giunta,[47] G. Giurgiu,[12] V. Glagolev,[15] D. Glenzinski,[17] M. Gold,[38] N. Goldschmidt,[18] J. Goldstein^{b},[43] A. Golossanov,[17] G. Gomez,[11] G. Gomez-Ceballos,[11] M. Goncharov,[54] O. González,[32] I. Gorelov,[38] A.T. Goshaw,[16] K. Goulianos,[51] A. Gresele,[44] M. Griffiths,[30] S. Grinstein,[22] C. Grosso-Pilcher,[13] R.C. Group,[18] U. Grundler,[24] J. Guimaraes da Costa,[22] Z. Gunay-Unalan,[36] C. Haber,[29] K. Hahn,[33] S.R. Hahn,[17] E. Halkiadakis,[53] A. Hamilton,[34] B.-Y. Han,[50] J.Y. Han,[50] R. Handler,[60] F. Happacher,[19] K. Hara,[56] M. Hare,[57] S. Harper,[43] R.F. Harr,[59] R.M. Harris,[17] M. Hartz,[48] K. Hatakeyama,[51] J. Hauser,[8] A. Heijboer,[46] B. Heinemann,[30] J. Heinrich,[46] C. Henderson,[33] M. Herndon,[60] J. Heuser,[26] D. Hidas,[16] C.S. Hill^{b},[10] D. Hirschbuehl,[26] A. Hocker,[17] A. Holloway,[22] S. Hou,[1] M. Houlden,[30] S.-C. Hsu,[9] B.T. Huffman,[43] R.E. Hughes,[40] U. Husemann,[61] J. Huston,[36] J. Incandela,[10] G. Introzzi,[47] M. Iori,[52] Y. Ishizawa,[56] A. Ivanov,[7] B. Iyutin,[33] E. James,[17] D. Jang,[53] B. Jayatilaka,[35] D. Jeans,[52] H. Jensen,[17] E.J. Jeon,[28] S. Jindariani,[18] M. Jones,[49] K.K. Joo,[28] S.Y. Jun,[12] J.E. Jung,[28] T.R. Junk,[24] T. Kamon,[54] P.E. Karchin,[59] Y. Kato,[42] Y. Kemp,[26] R. Kephart,[17] U. Kerzel,[26] V. Khotilovich,[54] B. Kilminster,[40] D.H. Kim,[28] H.S. Kim,[28] J.E. Kim,[28] M.J. Kim,[12] S.B. Kim,[28] S.H. Kim,[56] Y.K. Kim,[13] N. Kimura,[56] L. Kirsch,[6] S. Klimenko,[18] M. Klute,[33] B. Knuteson,[33] B.R. Ko,[16] K. Kondo,[58] D.J. Kong,[28] J. Konigsberg,[18] A. Korytov,[18] A.V. Kotwal,[16] A. Kovalev,[46] A.C. Kraan,[46] J. Kraus,[24] I. Kravchenko,[33] M. Kreps,[26] J. Kroll,[46] N. Krumnack,[4] M. Kruse,[16] V. Krutelyov,[10] T. Kubo,[56] S. E. Kuhlmann,[2] T. Kuhr,[26] Y. Kusakabe,[58] S. Kwang,[13] A.T. Laasanen,[49] S. Lai,[34] S. Lami,[47] S. Lammel,[17] M. Lancaster,[31] R.L. Lander,[7] K. Lannon,[40] A. Lath,[53] G. Latino,[47] I. Lazzizzera,[44] T. LeCompte,[2] J. Lee,[50] J. Lee,[28] Y.J. Lee,[28] S.W. Lee^{n},[54] R. Lefèvre,[3] N. Leonardo,[33] S. Leone,[47] S. Levy,[13] J.D. Lewis,[17] C. Lin,[61] C.S. Lin,[17] M. Lindgren,[17] E. Lipeles,[9] A. Lister,[7] D.O. Litvintsev,[17] T. Liu,[17] N.S. Lockyer,[46] A. Loginov,[61] M. Loreti,[44] P. Loverre,[52] R.-S. Lu,[1] D. Lucchesi,[44] P. Lujan,[29] P. Lukens,[17] G. Lungu,[18] L. Lyons,[43] J. Lys,[29] R. Lysak,[14] E. Lytken,[49] P. Mack,[26] D. MacQueen,[34] R. Madrak,[17] K. Maeshima,[17] K. Makhoul,[33] T. Maki,[23] P. Maksimovic,[25] S. Malde,[43] G. Manca,[30] F. Margaroli,[5] R. Marginean,[17] C. Marino,[26] C.P. Marino,[24] A. Martin,[61] M. Martin,[25] V. Martin^{g},[21] M. Martínez,[3] T. Maruyama,[56] P. Mastrandrea,[52] T. Masubuchi,[56] H. Matsunaga,[56] M.E. Mattson,[59] R. Mazini,[34] P. Mazzanti,[5] K.S. McFarland,[50] P. McIntyre,[54] R. McNulty^{f},[30] A. Mehta,[30] P. Mehtala,[23] S. Menzemer^{h},[11] A. Menzione,[47] P. Merkel,[49] C. Mesropian,[51] A. Messina,[36] T. Miao,[17] N. Miladinovic,[6] J. Miles,[33] R. Miller,[36] C. Mills,[10] M. Milnik,[26] A. Mitra,[1] G. Mitselmakher,[18] A. Miyamoto,[27] S. Moed,[20] N. Moggi,[5] B. Mohr,[8]

R. Moore,[17] M. Morello,[47] P. Movilla Fernandez,[29] J. Mülmenstädt,[29] A. Mukherjee,[17] Th. Muller,[26] R. Mumford,[25] P. Murat,[17] J. Nachtman,[17] A. Nagano,[56] J. Naganoma,[58] I. Nakano,[41] A. Napier,[57] V. Necula,[18] C. Neu,[46] M.S. Neubauer,[9] J. Nielsen,[29] T. Nigmanov,[48] L. Nodulman,[2] O. Norniella,[3] E. Nurse,[31] S.H. Oh,[16] Y.D. Oh,[28] I. Oksuzian,[18] T. Okusawa,[42] R. Oldeman,[30] R. Orava,[23] K. Osterberg,[23] C. Pagliarone,[47] E. Palencia,[11] V. Papadimitriou,[17] A.A. Paramonov,[13] B. Parks,[40] S. Pashapour,[34] J. Patrick,[17] G. Pauletta,[55] M. Paulini,[12] C. Paus,[33] D.E. Pellett,[7] A. Penzo,[55] T.J. Phillips,[16] G. Piacentino,[47] J. Piedra,[45] L. Pinera,[18] K. Pitts,[24] C. Plager,[8] L. Pondrom,[60] X. Portell,[3] O. Poukhov,[15] N. Pounder,[43] F. Prakoshyn,[15] A. Pronko,[17] J. Proudfoot,[2] F. Ptohos[e],[19] G. Punzi,[47] J. Pursley,[25] J. Rademacker[b],[43] A. Rahaman,[48] N. Ranjan,[49] S. Rappoccio,[22] B. Reisert,[17] V. Rekovic,[38] P. Renton,[43] M. Rescigno,[52] S. Richter,[26] F. Rimondi,[5] L. Ristori,[47] A. Robson,[21] T. Rodrigo,[11] E. Rogers,[24] S. Rolli,[57] R. Roser,[17] M. Rossi,[55] R. Rossin,[18] A. Ruiz,[11] J. Russ,[12] V. Rusu,[13] H. Saarikko,[23] S. Sabik,[34] A. Safonov,[54] W.K. Sakumoto,[50] G. Salamanna,[52] O. Saltó,[3] D. Saltzberg,[8] C. Sánchez,[3] L. Santi,[55] S. Sarkar,[52] L. Sartori,[47] K. Sato,[17] P. Savard,[34] A. Savoy-Navarro,[45] T. Scheidle,[26] P. Schlabach,[17] E.E. Schmidt,[17] M.P. Schmidt,[61] M. Schmitt,[39] T. Schwarz,[7] L. Scodellaro,[11] A.L. Scott,[10] A. Scribano,[47] F. Scuri,[47] A. Sedov,[49] S. Seidel,[38] Y. Seiya,[42] A. Semenov,[15] L. Sexton-Kennedy,[17] A. Sfyrla,[20] M.D. Shapiro,[29] T. Shears,[30] P.F. Shepard,[48] D. Sherman,[22] M. Shimojima[k],[56] M. Shochet,[13] Y. Shon,[60] I. Shreyber,[37] A. Sidoti,[47] P. Sinervo,[34] A. Sisakyan,[15] J. Sjolin,[43] A.J. Slaughter,[17] J. Slaunwhite,[40] K. Sliwa,[57] J.R. Smith,[7] F.D. Snider,[17] R. Snihur,[34] M. Soderberg,[35] A. Soha,[7] S. Somalwar,[53] V. Sorin,[36] J. Spalding,[17] F. Spinella,[47] T. Spreitzer,[34] P. Squillacioti,[47] M. Stanitzki,[61] A. Staveris-Polykalas,[47] R. St. Denis,[21] B. Stelzer,[8] O. Stelzer-Chilton,[43] D. Stentz,[39] J. Strologas,[38] D. Stuart,[10] J.S. Suh,[28] A. Sukhanov,[18] H. Sun,[57] T. Suzuki,[56] A. Taffard,[24] R. Takashima,[41] Y. Takeuchi,[56] K. Takikawa,[56] M. Tanaka,[2] R. Tanaka,[41] M. Tecchio,[35] P.K. Teng,[1] K. Terashi,[51] J. Thom[d],[17] A.S. Thompson,[21] E. Thomson,[46] P. Tipton,[61] V. Tiwari,[12] S. Tkaczyk,[17] D. Toback,[54] S. Tokar,[14] K. Tollefson,[36] T. Tomura,[56] D. Tonelli,[47] S. Torre,[19] D. Torretta,[17] S. Tourneur,[45] W. Trischuk,[34] R. Tsuchiya,[58] S. Tsuno,[41] N. Turini,[47] F. Ukegawa,[56] T. Unverhau,[21] S. Uozumi,[56] D. Usynin,[46] S. Vallecorsa,[20] N. van Remortel,[23] A. Varganov,[35] E. Vataga,[38] F. Vázquez[i],[18] G. Velev,[17] G. Veramendi,[24] V. Veszpremi,[49] R. Vidal,[17] I. Vila,[11] R. Vilar,[11] T. Vine,[31] I. Vollrath,[34] I. Volobouev[n],[29] G. Volpi,[47] F. Würthwein,[9] P. Wagner,[54] R.G. Wagner,[2] R.L. Wagner,[17] J. Wagner,[26] W. Wagner,[26] R. Wallny,[8] S.M. Wang,[1] A. Warburton,[34] S. Waschke,[21] D. Waters,[31] M. Weinberger,[54] W.C. Wester III,[17] B. Whitehouse,[57] D. Whiteson,[46] A.B. Wicklund,[2] E. Wicklund,[17] G. Williams,[34] H.H. Williams,[46] P. Wilson,[17] B.L. Winer,[40] P. Wittich[d],[17] S. Wolbers,[17] C. Wolfe,[13] T. Wright,[35] X. Wu,[20] S.M. Wynne,[30] A. Yagil,[17] K. Yamamoto,[42] J. Yamaoka,[53] T. Yamashita,[41] C. Yang,[61] U.K. Yang[j],[13] Y.C. Yang,[28] W.M. Yao,[29] G.P. Yeh,[17] J. Yoh,[17] K. Yorita,[13] T. Yoshida,[42] G.B. Yu,[50] I. Yu,[28] S.S. Yu,[17] J.C. Yun,[17] L. Zanello,[52] A. Zanetti,[55] I. Zaw,[22] X. Zhang,[24] J. Zhou,[53] and S. Zucchelli[5]

(CDF Collaboration*)

[1] *Institute of Physics, Academia Sinica, Taipei, Taiwan 11529, Republic of China*
[2] *Argonne National Laboratory, Argonne, Illinois 60439*
[3] *Institut de Fisica d'Altes Energies, Universitat Autonoma de Barcelona, E-08193, Bellaterra (Barcelona), Spain*
[4] *Baylor University, Waco, Texas 76798*
[5] *Istituto Nazionale di Fisica Nucleare, University of Bologna, I-40127 Bologna, Italy*
[6] *Brandeis University, Waltham, Massachusetts 02254*
[7] *University of California, Davis, Davis, California 95616*
[8] *University of California, Los Angeles, Los Angeles, California 90024*
[9] *University of California, San Diego, La Jolla, California 92093*
[10] *University of California, Santa Barbara, Santa Barbara, California 93106*
[11] *Instituto de Fisica de Cantabria, CSIC-University of Cantabria, 39005 Santander, Spain*
[12] *Carnegie Mellon University, Pittsburgh, PA 15213*
[13] *Enrico Fermi Institute, University of Chicago, Chicago, Illinois 60637*
[14] *Comenius University, 842 48 Bratislava, Slovakia; Institute of Experimental Physics, 040 01 Kosice, Slovakia*
[15] *Joint Institute for Nuclear Research, RU-141980 Dubna, Russia*
[16] *Duke University, Durham, North Carolina 27708*
[17] *Fermi National Accelerator Laboratory, Batavia, Illinois 60510*
[18] *University of Florida, Gainesville, Florida 32611*

* With visitors from [a]University of Athens, [b]University of Bristol, [c]University Libre de Bruxelles, [d]Cornell University, [e]University of Cyprus, [f]University of Dublin, [g]University of Edinburgh, [h]University of Heidelberg, [i]Universidad Iberoamericana, [j]University of Manchester, [k]Nagasaki Institute of Applied Science, [l]University de Oviedo, [m]University of London, Queen Mary and Westfield College, [n]Texas Tech University, [o]IFIC(CSIC-Universitat de Valencia),

[19] Laboratori Nazionali di Frascati, Istituto Nazionale di Fisica Nucleare, I-00044 Frascati, Italy
[20] University of Geneva, CH-1211 Geneva 4, Switzerland
[21] Glasgow University, Glasgow G12 8QQ, United Kingdom
[22] Harvard University, Cambridge, Massachusetts 02138
[23] Division of High Energy Physics, Department of Physics,
University of Helsinki and Helsinki Institute of Physics, FIN-00014, Helsinki, Finland
[24] University of Illinois, Urbana, Illinois 61801
[25] The Johns Hopkins University, Baltimore, Maryland 21218
[26] Institut für Experimentelle Kernphysik, Universität Karlsruhe, 76128 Karlsruhe, Germany
[27] High Energy Accelerator Research Organization (KEK), Tsukuba, Ibaraki 305, Japan
[28] Center for High Energy Physics: Kyungpook National University,
Taegu 702-701, Korea; Seoul National University, Seoul 151-742,
Korea; and SungKyunKwan University, Suwon 440-746, Korea
[29] Ernest Orlando Lawrence Berkeley National Laboratory, Berkeley, California 94720
[30] University of Liverpool, Liverpool L69 7ZE, United Kingdom
[31] University College London, London WC1E 6BT, United Kingdom
[32] Centro de Investigaciones Energeticas Medioambientales y Tecnologicas, E-28040 Madrid, Spain
[33] Massachusetts Institute of Technology, Cambridge, Massachusetts 02139
[34] Institute of Particle Physics: McGill University, Montréal,
Canada H3A 2T8; and University of Toronto, Toronto, Canada M5S 1A7
[35] University of Michigan, Ann Arbor, Michigan 48109
[36] Michigan State University, East Lansing, Michigan 48824
[37] Institution for Theoretical and Experimental Physics, ITEP, Moscow 117259, Russia
[38] University of New Mexico, Albuquerque, New Mexico 87131
[39] Northwestern University, Evanston, Illinois 60208
[40] The Ohio State University, Columbus, Ohio 43210
[41] Okayama University, Okayama 700-8530, Japan
[42] Osaka City University, Osaka 588, Japan
[43] University of Oxford, Oxford OX1 3RH, United Kingdom
[44] University of Padova, Istituto Nazionale di Fisica Nucleare,
Sezione di Padova-Trento, I-35131 Padova, Italy
[45] LPNHE, Universite Pierre et Marie Curie/IN2P3-CNRS, UMR7585, Paris, F-75252 France
[46] University of Pennsylvania, Philadelphia, Pennsylvania 19104
[47] Istituto Nazionale di Fisica Nucleare Pisa, Universities of Pisa,
Siena and Scuola Normale Superiore, I-56127 Pisa, Italy
[48] University of Pittsburgh, Pittsburgh, Pennsylvania 15260
[49] Purdue University, West Lafayette, Indiana 47907
[50] University of Rochester, Rochester, New York 14627
[51] The Rockefeller University, New York, New York 10021
[52] Istituto Nazionale di Fisica Nucleare, Sezione di Roma 1,
University of Rome "La Sapienza," I-00185 Roma, Italy
[53] Rutgers University, Piscataway, New Jersey 08855
[54] Texas A&M University, College Station, Texas 77843
[55] Istituto Nazionale di Fisica Nucleare, University of Trieste/ Udine, Italy
[56] University of Tsukuba, Tsukuba, Ibaraki 305, Japan
[57] Tufts University, Medford, Massachusetts 02155
[58] Waseda University, Tokyo 169, Japan
[59] Wayne State University, Detroit, Michigan 48201
[60] University of Wisconsin, Madison, Wisconsin 53706
[61] Yale University, New Haven, Connecticut 06520

(Dated: February 7, 2008)

We report on measurements of the inclusive jet production cross section as a function of the jet transverse momentum in $p\overline{p}$ collisions at $\sqrt{s} = 1.96$ TeV, using the k_{T} algorithm and a data sample corresponding to 1.0 fb^{-1} collected with the Collider Detector at Fermilab in Run II. The measurements are carried out in five different jet rapidity regions with $|y^{\mathrm{jet}}| < 2.1$ and transverse momentum in the range $54 < p_{\mathrm{T}}^{\mathrm{jet}} < 700$ GeV/c. Next-to-leading order perturbative QCD predictions are in good agreement with the measured cross sections.

PACS numbers: PACS numbers 12.38.Aw, 13.85.-t, 13.87.-a

I. INTRODUCTION

The measurement of the inclusive jet cross section as a function of the jet transverse momentum, $p_{\rm T}^{\rm jet}$, in $p\overline{p}$ collisions at $\sqrt{s} = 1.96$ TeV constitutes a test of perturbative quantum chromodynamics (pQCD) [1]. In Run II of the Tevatron, measurements of the jet cross section for jets with $p_{\rm T}^{\rm jet}$ up to about 700 GeV/c [2, 3] have extended the $p_{\rm T}^{\rm jet}$ range by more than 150 GeV/c compared to Run I [4–6]. In particular, the CDF collaboration recently published results [2] on inclusive jet production using the $k_{\rm T}$ algorithm [7, 8] for jets with $p_{\rm T}^{\rm jet} > 54$ GeV/c and rapidity [9] in the region $0.1 < |y^{\rm jet}| < 0.7$, which are well described by next-to-leading order (NLO) pQCD predictions [10]. As discussed in [2], the $k_{\rm T}$ algorithm has been widely used for precise QCD measurements at both e^+e^- and $e^{\pm}p$ colliders, and makes possible a well defined comparison to the theoretical predictions [8]. The pQCD calculations involve matrix elements, describing the hard interaction between partons, convoluted with parton density functions (PDFs) [11, 12] in the proton and antiproton that require input from experiment. The pQCD predictions are affected by the still-limited knowledge of the gluon PDF, which translates into a large uncertainty on the theoretical cross sections at high $p_{\rm T}^{\rm jet}$ [2, 3]. Inclusive jet cross section measurements from Run I at the Tevatron [5], performed in different jet rapidity regions, have been used to partially constrain the gluon distribution in the proton. This article continues the studies on jet production using the $k_{\rm T}$ algorithm at the Tevatron [2, 6] and presents new measurements of the inclusive jet production cross section as a function of $p_{\rm T}^{\rm jet}$ in five different jet rapidity regions up to $|y^{\rm jet}| = 2.1$, based on 1.0 fb^{-1} of CDF Run II data. The measurements are corrected to the hadron level [13] and compared to NLO pQCD predictions.

II. EXPERIMENTAL SETUP

The CDF II detector (see Fig. 1) is described in detail in [14]. The sub-detectors most relevant for this analysis are discussed briefly here. The detector has a charged particle tracking system immersed in a 1.4 T magnetic field. A silicon microstrip detector [15] provides tracking over the radial range 1.35 to 28 cm and covers the pseudorapidity range $|\eta| < 2$. A 3.1-m-long open-cell drift chamber [16] covers the radial range from 44 to 132 cm and provides tracking coverage for $|\eta| < 1$. Segmented sampling calorimeters, arranged in a projective tower geometry, surround the tracking system and measure the energy of interacting particles for $|\eta| < 3.6$. The central barrel calorimeter [17] covers the region $|\eta| < 1$. It consists of two sections, an electromagnetic calorimeter (CEM) and a hadronic calorimeter (CHA), divided into 480 towers of size 0.1 in η and 15^o in ϕ. The end-wall hadronic calorimeter (WHA) [18] is behind the central barrel calorimeter in the region $0.6 < |\eta| < 1.0$, providing forward coverage out to $|\eta| < 1.3$. In Run II, new forward scintillator-plate calorimeters [19] replaced the Run I gas calorimeter system. The new plug electromagnetic calorimeter (PEM) covers the region $1.1 < |\eta| < 3.6$, while the new hadronic calorimeter (PHA) provides coverage in the $1.3 < |\eta| < 3.6$ region. The calorimeter has gaps at $|\eta| \approx 0$ (between the two halves of the central barrel calorimeter) and at $|\eta| \approx 1.1$ (in the region between the WHA and the plug calorimeters). The measured energy resolutions for electrons in the electromagnetic calorimeters [17, 19] are $14\%/\sqrt{E_T} \oplus 2\%$ (CEM) and $16\%/\sqrt{E} \oplus 1\%$ (PEM), where the energies are expressed in GeV. The single-pion energy resolutions in the hadronic calorimeters, as determined in test-beam data [17–19], are $50\%/\sqrt{E_T} \oplus 3\%$ (CHA), $75\%/\sqrt{E_T} \oplus 4\%$ (WHA) and $80\%/\sqrt{E} \oplus 5\%$ (PHA). Cherenkov counters covering the $3.7 < |\eta| < 4.7$ region [20] measure the average number of inelastic $p\overline{p}$ collisions per bunch crossing and thereby determine the beam luminosity.

III. JET RECONSTRUCTION

The $k_{\rm T}$ algorithm [8] is used to reconstruct jets from the energy depositions in the calorimeter towers in both data and Monte Carlo simulated events (see Section VI). For each calorimeter tower, the four-momenta [21] of its electromagnetic and hadronic sections are summed to define a physics tower. First, all physics towers with transverse momentum above 0.1 GeV/c are considered as protojets. The quantities

$$k_{\rm T,i} = p_{\rm T,i}^2 \quad ; \quad k_{\rm T,(i,j)} = min(p_{\rm T,i}^2, p_{\rm T,j}^2) \cdot \Delta R_{\rm i,j}^2 / D^2, \tag{1}$$

are computed for each protojet and pair of protojets, respectively, where $p_{\rm T,i}$ denotes the transverse momentum of the i$^{\rm th}$ protojet, $\Delta R_{\rm i,j}$ is the distance ($y - \phi$ space) between each pair of protojets, and D is a parameter that approximately controls the size of the jet by limiting, in each iteration, the clustering of protojets according to their spacial separation. All $k_{\rm T,i}$ and $k_{\rm T,(i,j)}$ values are then collected into a single sorted list. In this list, if the smallest quantity is of the type $k_{\rm T,i}$, the corresponding protojet is promoted to be a jet and removed from the list. Otherwise, if

the smallest quantity is of the type $k_{\mathrm{T,(i,j)}}$, the protojets are combined into a single protojet by summing up their four-vector components. The procedure is iterated over protojets until the list is empty. The jet transverse momentum, rapidity, and azimuthal angle are denoted as $p_{\mathrm{T,cal}}^{\mathrm{jet}}$, $y_{\mathrm{cal}}^{\mathrm{jet}}$, and $\phi_{\mathrm{cal}}^{\mathrm{jet}}$, respectively.

In the Monte Carlo event samples, the same jet algorithm is also applied to the final-state particles, considering all particles as protojets, to search for jets at the hadron level. The resulting hadron-level jet variables are denoted as $p_{\mathrm{T,had}}^{\mathrm{jet}}$, $y_{\mathrm{had}}^{\mathrm{jet}}$, and $\phi_{\mathrm{had}}^{\mathrm{jet}}$.

IV. EVENT SELECTION

Events are selected online using a three-level trigger system [22] with unique sets of selection criteria called paths. For the different trigger paths used in this measurement, this selection is based on the measured energy deposits in the calorimeter towers, with different thresholds on the jet E_T and different prescale factors [23] (see Table I). In the first-level trigger, a single trigger tower [24] with E_T above 5 GeV or 10 GeV, depending on the trigger path, is required. In the second-level trigger, calorimeter clusters are formed around the selected trigger towers. The events are required to have at least one second-level trigger cluster with E_T above a given threshold, which varies between 15 and 90 GeV for the different trigger paths. In the third-level trigger, jets are reconstructed using the CDF Run I cone algorithm [25], and the events are required to have at least one jet with E_T above 20 to 100 GeV.

Trigger Path	Level 1 tower E_T [GeV]	Level 2 cluster E_T [GeV]	Level 3 jet E_T [GeV]	eff. prescale
JET 20	5	15	20	775
JET 50	5	40	50	34
JET 70	10	60	70	8
JET 100	10	90	100	1

TABLE I: Summary of trigger paths, trigger thresholds and effective prescale factors employed to collect the data.

Jets are then reconstructed using the k_{T} algorithm, as explained in Section III, with $D = 0.7$. For each trigger path, the minimum $p_{\mathrm{T,cal}}^{\mathrm{jet}}$, in each $|y_{\mathrm{cal}}^{\mathrm{jet}}|$ region, is chosen in such a way that the trigger selection is fully efficient. The efficiency for a given trigger path is obtained using events from a different trigger path with lower transverse energy thresholds (see Table I). In the case of the JET 20 trigger path, the trigger efficiency is extracted from additional control samples, which include a sample with only first-level trigger requirements as well as data collected using unbiased trigger paths with no requirement on the energy deposits in the calorimeter towers. As an example, for jets in the region $0.1 < |y_{\mathrm{cal}}^{\mathrm{jet}}| < 0.7$, Fig. 2 shows the trigger efficiency as a function of $p_{\mathrm{T,cal}}^{\mathrm{jet}}$ for the different samples. The following selection criteria have been imposed:

1. Events are required to have at least one reconstructed primary vertex with z-position within 60 cm of the nominal interaction point. This partially removes beam-related backgrounds and ensures a well-understood event-by-event jet kinematics.

2. Events are required to have at least one jet with rapidity in the region $|y_{\mathrm{cal}}^{\mathrm{jet}}| < 2.1$ and corrected $p_{\mathrm{T,cal}}^{\mathrm{jet}}$ (see Section IX) above 54 GeV/c, which constitutes the minimum jet transverse momentum considered in the analysis. The measurements are limited to jets with $|y_{\mathrm{cal}}^{\mathrm{jet}}| < 2.1$ to avoid contributions from the p and $\overline{p}$ remnants that would affect the measured $p_{\mathrm{T,cal}}^{\mathrm{jet}}$ in the most forward region of the calorimeter.

3. In order to remove beam-related backgrounds and cosmic rays, the events are required to fulfill $\not\!\!E_T/\sqrt{\Sigma E_T} < F(p_{\mathrm{T,cal}}^{\mathrm{jet1}})$, where $\not\!\!E_T$ denotes the missing transverse energy [26] and $\Sigma E_T = \sum_i E_T^i$ is the total transverse energy of the event, as measured using calorimeter towers with E_T^i above 0.1 GeV. The threshold function $F(p_{\mathrm{T,cal}}^{\mathrm{jet1}})$ is defined as $F(p_{\mathrm{T}}^{\mathrm{jet}}) = min(2{+}0.0125{\times}p_{\mathrm{T}}^{\mathrm{jet}}, 7)$, where $p_{\mathrm{T,cal}}^{\mathrm{jet1}}$ is the uncorrected transverse momentum of the leading jet (highest $p_{\mathrm{T}}^{\mathrm{jet}}$) in GeV/$c$, and F is in GeV$^{1/2}$. This criterion preserves more than 95% of the QCD events, as determined from Monte Carlo studies (see Section VI). A visual scan of events with $p_{\mathrm{T,cal}}^{\mathrm{jet}} > 400$ GeV/c did not show remaining backgrounds.

Measurements are carried out in five different jet rapidity regions: $|y_{\mathrm{cal}}^{\mathrm{jet}}| < 0.1$, $0.1 < |y_{\mathrm{cal}}^{\mathrm{jet}}| < 0.7$, $0.7 < |y_{\mathrm{cal}}^{\mathrm{jet}}| < 1.1$, $1.1 < |y_{\mathrm{cal}}^{\mathrm{jet}}| < 1.6$, and $1.6 < |y_{\mathrm{cal}}^{\mathrm{jet}}| < 2.1$, where the different boundaries are chosen to reduce systematic effects coming from the layout of the calorimeter system.

V. EFFECT OF MULTIPLE $P\overline{P}$ INTERACTIONS

The measured $p_{\mathrm{T,cal}}^{\mathrm{jet}}$ includes contributions from multiple $p\overline{p}$ interactions per bunch crossing at high instantaneous luminosity, $\mathcal{L}^{\mathrm{inst}}$. The data used in this measurement were collected at $\mathcal{L}^{\mathrm{inst}}$ between $0.2 \times 10^{31}\mathrm{cm}^{-2}\mathrm{s}^{-1}$ and $16.3 \times 10^{31}\mathrm{cm}^{-2}\mathrm{s}^{-1}$ with an average of $4.1 \times 10^{31}\mathrm{cm}^{-2}\mathrm{s}^{-1}$. On average, 1.5 inelastic $p\overline{p}$ interactions per bunch crossing are expected. At the highest $\mathcal{L}^{\mathrm{inst}}$ considered, an average of 5.9 interactions per bunch crossing are produced. This mainly affects the measured cross section at low $p_{\mathrm{T}}^{\mathrm{jet}}$ where the contributions are sizeable. Multiple interactions are identified via the presence of additional primary vertices reconstructed from charged particles. The measured jet transverse momenta are corrected for this effect by removing a certain amount of transverse momentum, $\delta_{p_{\mathrm{T}}}^{\mathrm{mi}} \times (N_{\mathrm{V}} - 1)$, where N_{V} denotes the number of reconstructed primary vertices in the event and $\delta_{p_{\mathrm{T}}}^{\mathrm{mi}}$ is determined from the data by requiring that, after the correction is applied, the ratio of cross sections at low and high $\mathcal{L}^{\mathrm{inst}}$ does not show any $p_{\mathrm{T}}^{\mathrm{jet}}$ dependence. The study is carried out separately in each $|y_{\mathrm{cal}}^{\mathrm{jet}}|$ region, and the results are consistent with a common value $\delta_{p_{\mathrm{T}}}^{\mathrm{mi}} = 1.86 \pm 0.23$ GeV/c across the whole rapidity range.

VI. MONTE CARLO SIMULATION

Monte Carlo simulated event samples are used to determine the response of the detector and the correction factors to the hadron level. The generated samples are passed through a full CDF II detector simulation (based on GEANT3 [27], where the GFLASH [28] package is used to simulate the energy deposition in the calorimeters) and then reconstructed and analyzed using the same analysis chain as used for the data.

Samples of simulated inclusive jet events have been generated with PYTHIA 6.203 [29] and HERWIG 6.4 [30] Monte Carlo generators, using CTEQ5L [31] PDFs. The PYTHIA samples have been created using a specially tuned set of parameters, denoted as PYTHIA-TUNE A [32], that includes enhanced contributions from initial-state gluon radiation and secondary parton interactions between remnants. The parameters were determined from dedicated studies of the underlying event using the CDF Run I data [33] and has been shown to properly describe the measured jet shapes in Run II [34]. In the case of PYTHIA, fragmentation into hadrons is carried out using the string model [35] as implemented in JETSET [36], while HERWIG implements the cluster model [37].

VII. SIMULATION OF THE CALORIMETER RESPONSE TO JETS

Dedicated studies have been performed to validate the Monte Carlo simulation of the calorimeter response to jets for the different $|y_{\mathrm{cal}}^{\mathrm{jet}}|$ regions. Previous analyses [2] for jets with $0.1 < |y_{\mathrm{cal}}^{\mathrm{jet}}| < 0.7$ indicate that the simulation properly reproduces both the average $p_{\mathrm{T}}^{\mathrm{jet}}$ and the jet momentum resolution, $\sigma_{p_{\mathrm{T}}^{\mathrm{jet}}}$, as measured in the data. The study is performed for the rest of the $|y_{\mathrm{cal}}^{\mathrm{jet}}|$ regions using jets in the range $0.1 < |y_{\mathrm{cal}}^{\mathrm{jet}}| < 0.7$ as a reference. An exclusive dijet sample is selected, in data and simulated events, with the following criteria:

1. Events are required to have one and only one reconstructed primary vertex with z-position within 60 cm of the nominal interaction point.
2. Events are required to have exactly two jets with $p_{\mathrm{T,cal}}^{\mathrm{jet}} > 10$ GeV/c, where one of the jets must be in the region $0.1 < |y_{\mathrm{cal}}^{\mathrm{jet}}| < 0.7$.
3. $\not\!\!E_T/\sqrt{\Sigma E_T} < F(p_{\mathrm{T,cal}}^{\mathrm{jet1}})$, as explained in Section IV.

The bisector method [38] is applied to data and simulated exclusive dijet events to test the accuracy of the simulated $\sigma_{p_{\mathrm{T}}^{\mathrm{jet}}}$ in the detector. The study indicates that the simulation systematically underestimates the measured $\sigma_{p_{\mathrm{T}}^{\mathrm{jet}}}$ by 6% and 10% for jets in the regions $0.7 < |y_{\mathrm{cal}}^{\mathrm{jet}}| < 1.1$ and $1.6 < |y_{\mathrm{cal}}^{\mathrm{jet}}| < 2.1$, respectively, with no significant $p_{\mathrm{T,cal}}^{\mathrm{jet}}$ dependence. An additional smearing of the reconstructed $p_{\mathrm{T,cal}}^{\mathrm{jet}}$ is applied to the simulated events to account for this effect. In the region $1.1 < |y_{\mathrm{cal}}^{\mathrm{jet}}| < 1.6$, the measured $\sigma_{p_{\mathrm{T}}^{\mathrm{jet}}}$ is overestimated by 5% in the simulation. The effect on the final result is included via slightly modified unfolding factors (see Section IX). For jets with $|y_{\mathrm{cal}}^{\mathrm{jet}}| < 0.1$, the simulation properly describes the measured $\sigma_{p_{\mathrm{T}}^{\mathrm{jet}}}$. Figure 3 shows the ratio between $\sigma_{p_{\mathrm{T}}^{\mathrm{jet}}}$ in data and simulated events, $\sigma_{p_{\mathrm{T}}^{\mathrm{jet}}}^{\mathrm{data}}/\sigma_{p_{\mathrm{T}}^{\mathrm{jet}}}^{\mathrm{mc}}$, in different $|y_{\mathrm{cal}}^{\mathrm{jet}}|$ regions as a function of the average $p_{\mathrm{T,cal}}^{\mathrm{jet}}$ of the dijet event. After corrections have been applied to the simulated events, data and simulation agree. In the region $1.1 < |y_{\mathrm{cal}}^{\mathrm{jet}}| < 1.6$, and only for the

purpose of presentation, a 5% smearing of the reconstructed $p_{\rm T,cal}^{\rm jet}$ is applied to the data to show the resulting good agreement with the uncorrected simulated resolution. The relative difference between data and simulated resolutions is conservatively taken to be $\pm 8\%$ (see Fig. 3) over the whole range in $p_{\rm T,cal}^{\rm jet}$ and $|y_{\rm cal}^{\rm jet}|$ in the evaluation of systematic uncertainties.

The average jet momentum calorimeter response in the simulation is then tested by comparing the $p_{\rm T,cal}^{\rm jet}$ balance in data and simulated exclusive dijet events. The variable β, defined as [39]

$$\beta = \frac{1+\langle\Delta\rangle}{1-\langle\Delta\rangle}\ , \quad \text{with} \quad \Delta = \frac{p_{\rm T,cal}^{\text{test jet}} - p_{\rm T,cal}^{\text{ref. jet}}}{p_{\rm T,cal}^{\text{test jet}} + p_{\rm T,cal}^{\text{ref. jet}}}\ , \tag{2}$$

is computed in data and simulated events in bins of $(p_{\rm T,cal}^{\text{test jet}} + p_{\rm T,cal}^{\text{ref. jet}})/2$, where $p_{\rm T,cal}^{\text{ref. jet}}$ denotes the transverse momentum of the jet in the region $0.1 < |y_{\rm cal}^{\rm jet}| < 0.7$, and $p_{\rm T,cal}^{\text{test jet}}$ is the transverse momentum of the jet in the $|y_{\rm cal}^{\rm jet}|$ region under study. Figure 4 presents the ratios $\beta_{\rm data}/\beta_{\rm mc}$ as a function of $p_{\rm T,cal}^{\rm jet} = p_{\rm T,cal}^{\text{test jet}}$ in the different $|y_{\rm cal}^{\rm jet}|$ bins. The study indicates that small corrections are required around calorimeter gaps, $|y_{\rm cal}^{\rm jet}| < 0.1$ and $1.1 < |y_{\rm cal}^{\rm jet}| < 1.6$, as well as in the most forward region, $1.6 < |y_{\rm cal}^{\rm jet}| < 2.1$. For jets with $|y_{\rm cal}^{\rm jet}| > 1.1$, the correction shows a moderate $p_{\rm T,cal}^{\rm jet}$ dependence, and several parameterizations are considered to extrapolate to very high $p_{\rm T,cal}^{\rm jet}$. The difference observed in the final results, using different parameterizations, is included as part of the total systematic uncertainty.

VIII. RECONSTRUCTION OF THE JET VARIABLES

The jet reconstruction in the detector is studied using Monte Carlo event samples, with modified jet energy response in the calorimeter, as described in the previous section, and pairs of jets at the calorimeter and hadron levels matched in (y - ϕ) space by requiring $\sqrt{(y_{\rm cal}^{\rm jet} - y_{\rm had}^{\rm jet})^2 + (\phi_{\rm cal}^{\rm jet} - \phi_{\rm had}^{\rm jet})^2} < D$. These studies indicate that the angular variables of a jet are reconstructed with no significant systematic shift and with a resolution better than 0.05 units in y and ϕ at low $p_{\rm T,cal}^{\rm jet}$, improving as $p_{\rm T,cal}^{\rm jet}$ increases. The measured $p_{\rm T,cal}^{\rm jet}$ systematically underestimates that of the hadron level jet. This is attributed mainly to the non-compensating nature of the calorimeter [17]. For jets with $p_{\rm T,cal}^{\rm jet}$ around 50 GeV/c, the jet transverse momentum is reconstructed with an average shift that varies between -9% and -30% and a resolution between 10% and 16%, depending on the $|y_{\rm cal}^{\rm jet}|$ region. The jet reconstruction improves as $p_{\rm T,cal}^{\rm jet}$ increases. For jets with $p_{\rm T,cal}^{\rm jet}$ around 500 GeV/c, the average shift is -7% and the resolution is about 7%.

IX. UNFOLDING

The measured $p_{\rm T,cal}^{\rm jet}$ distributions in the different $|y_{\rm cal}^{\rm jet}|$ regions are unfolded back to the hadron level using simulated event samples (see Section VI), after including the modified jet energy response described in Section VII. PYTHIA-TUNE A provides a reasonable description of the different jet and underlying event quantities, and is used to determine the correction factors in the unfolding procedure. In order to avoid any potential bias on the correction factors due to the particular PDF set used during the generation of the simulated samples, which translates into slightly different simulated $p_{\rm T,cal}^{\rm jet}$ distributions, the underlying $\hat{p}_t$ spectrum [40] in PYTHIA-TUNE A is re-weighted until the Monte Carlo samples accurately follow each of the measured $p_{\rm T,cal}^{\rm jet}$ distributions. The unfolding is carried out in two steps.

First, an average correction is computed separately in each jet rapidity region using corresponding matched pairs of jets at the calorimeter and hadron levels. The correlation $\langle p_{\rm T,had}^{\rm jet} - p_{\rm T,cal}^{\rm jet}\rangle$ versus $\langle p_{\rm T,cal}^{\rm jet}\rangle$ (see Fig. 5), computed in bins of $(p_{\rm T,had}^{\rm jet} + p_{\rm T,cal}^{\rm jet})/2$, is used to extract correction factors which are then applied to the measured jets to obtain the corrected transverse momenta, $p_{\rm T,cor}^{\rm jet}$. In each jet rapidity region, a cross section is defined as

$$\frac{d^2\sigma}{dp_{\rm T,cor}^{\rm jet} dy_{\rm cal}^{\rm jet}} = \frac{1}{\mathcal{L}} \frac{N_{\rm cor}^{\rm jet}}{\Delta p_{\rm T,cor}^{\rm jet}\ \Delta y_{\rm cal}^{\rm jet}}, \tag{3}$$

where $N_{\rm cor}^{\rm jet}$ denotes the number of jets in a given $p_{\rm T,cor}^{\rm jet}$ bin, $\Delta p_{\rm T,cor}^{\rm jet}$ is the size of the bin, $\Delta y_{\rm cal}^{\rm jet}$ denotes the size of the region in $y_{\rm cal}^{\rm jet}$, and $\mathcal{L}$ is the integrated luminosity. $N_{\rm cor}^{\rm jet}$ includes event-by-event weights that account for trigger prescale factors, and $\Delta p_{\rm T,cor}^{\rm jet}$ is chosen according to the jet momentum resolution.

Second, each measurement is corrected for acceptance and smearing effects using a bin-by-bin unfolding procedure, which also accounts for the efficiency of the selection criteria. The unfolding factors, defined as

$$U(p_{\mathrm{T,cor}}^{\mathrm{jet}}, y_{\mathrm{cal}}^{\mathrm{jet}}) = \frac{d^2\sigma/dp_{\mathrm{T,had}}^{\mathrm{jet}}dy_{\mathrm{had}}^{\mathrm{jet}}}{d^2\sigma/dp_{\mathrm{T,cor}}^{\mathrm{jet}}dy_{\mathrm{cal}}^{\mathrm{jet}}}, \tag{4}$$

are extracted from Monte Carlo event samples and applied to the measured $p_{\mathrm{T,cor}}^{\mathrm{jet}}$ distributions to obtain the final results. As shown in Fig. 6, the factor $U(p_{\mathrm{T,cor}}^{\mathrm{jet}}, y_{\mathrm{cal}}^{\mathrm{jet}})$ increases with $p_{\mathrm{T,cor}}^{\mathrm{jet}}$ and presents a moderate $|y_{\mathrm{cal}}^{\mathrm{jet}}|$ dependence. At low $p_{\mathrm{T,cor}}^{\mathrm{jet}}$, the unfolding factor varies between 1.02 and 1.06 for different rapidity regions. For jets with $p_{\mathrm{T,cor}}^{\mathrm{jet}}$ of about 300 GeV/c, the factor varies between 1.1 and 1.2, and increases up to 1.3 - 1.4 at very high $p_{\mathrm{T,cor}}^{\mathrm{jet}}$. In the region $1.1 < |y_{\mathrm{cal}}^{\mathrm{jet}}| < 1.6$, the unfolding factor includes an additional correction, $f_{\mathrm{U}}(p_{\mathrm{T,cor}}^{\mathrm{jet}})$, to account for the fact that the simulation overestimates the jet momentum resolution in that region (see Section VII). The factor $f_{\mathrm{U}}(p_{\mathrm{T,cor}}^{\mathrm{jet}})$ is computed from Monte Carlo samples as the ratio between the $p_{\mathrm{T,had}}^{\mathrm{jet}}$ distribution smeared using the simulated $\sigma_{p_{\mathrm{T}}^{\mathrm{jet}}}$ and the one smeared using $\sigma_{p_{\mathrm{T}}^{\mathrm{jet}}}$ in data as extracted from the bisector method (see Section VII). The factor $f_{\mathrm{U}}(p_{\mathrm{T,cor}}^{\mathrm{jet}})$ is about 1.03 and shows no significant $p_{\mathrm{T,cor}}^{\mathrm{jet}}$ dependence.

X. SYSTEMATIC UNCERTAINTIES

A detailed study of the systematic uncertainties on the measurements has been carried out [41]. Tables II-III show the different contributions to the total systematic uncertainty in each $p_{\mathrm{T}}^{\mathrm{jet}}$ bin and $|y^{\mathrm{jet}}|$ region:

1. The measured jet energies are varied by ±2% at low $p_{\mathrm{T}}^{\mathrm{jet}}$ to ±2.7% at high $p_{\mathrm{T}}^{\mathrm{jet}}$ to account for the uncertainty on the absolute energy scale in the calorimeter [42]. This introduces an uncertainty on the measured cross sections which varies between ±9% at low $p_{\mathrm{T}}^{\mathrm{jet}}$ and $^{+61\%}_{-39\%}$ at high $p_{\mathrm{T}}^{\mathrm{jet}}$, and dominates the total systematic uncertainty on the different measurements.

2. Several sources of systematic uncertainty on the ratio $\beta_{\mathrm{data}}/\beta_{\mathrm{mc}}$ are considered for the different $|y^{\mathrm{jet}}|$ regions:

   (a) The uncertainty on the definition of the exclusive dijet sample in data and Monte Carlo events introduces a ±0.5% uncertainty on the absolute energy scale for jets outside the region $0.1 < |y^{\mathrm{jet}}| < 0.7$, which translates into an uncertainty on the cross sections between ±2% at low $p_{\mathrm{T}}^{\mathrm{jet}}$ and ±10% at very high $p_{\mathrm{T}}^{\mathrm{jet}}$.

   (b) The use of different $\beta_{\mathrm{data}}/\beta_{\mathrm{mc}}$ parameterizations for jets with $|y^{\mathrm{jet}}| > 1.1$ introduces uncertainties between 12% and 23% at very high $p_{\mathrm{T}}^{\mathrm{jet}}$.

   (c) In the region $1.1 < |y^{\mathrm{jet}}| < 1.6$, an additional $^{+0\%}_{-3\%}$ uncertainty on the measured cross sections, independent of $p_{\mathrm{T}}^{\mathrm{jet}}$, accounts for variations in the $\beta_{\mathrm{data}}/\beta_{\mathrm{mc}}$ ratio due to the overestimation of the jet momentum resolution in the simulated samples.

3. A ±8% uncertainty on the jet momentum resolution introduces an uncertainty between ±2% at low $p_{\mathrm{T}}^{\mathrm{jet}}$ and $^{+12\%}_{-9\%}$ at high $p_{\mathrm{T}}^{\mathrm{jet}}$.

4. The unfolding procedure is repeated using HERWIG instead of PYTHIA-TUNE A to account for the uncertainty on the modeling of the parton cascades and the jet fragmentation into hadrons. This translates into an uncertainty on the measured cross sections between ±3% and ±8% at low $p_{\mathrm{T}}^{\mathrm{jet}}$ that becomes negligible at very high $p_{\mathrm{T}}^{\mathrm{jet}}$.

5. The unfolding procedure is also carried out using unweighted PYTHIA-TUNE A, to estimate the residual dependence on the $p_{\mathrm{T}}^{\mathrm{jet}}$ spectra. This introduces an uncertainty of about ±3% to ±7% at very high $p_{\mathrm{T}}^{\mathrm{jet}}$, which becomes negligible at low $p_{\mathrm{T}}^{\mathrm{jet}}$.

6. The quoted ±0.23 GeV/c uncertainty on $\delta_{p_{\mathrm{T}}}^{\mathrm{mi}}$ is taken into account. The maximal effect on the measured cross sections is about ±2%.

7. Different sources of systematic uncertainty related to the selection criteria are considered. The threshold on the z-position of the primary vertex is varied by ±5 cm in data and simulated events. The lower edge of each $p_{\mathrm{T,cal}}^{\mathrm{jet}}$ bin is varied by ±3% in data and simulated events. The $\not\!\!E_T$ scale is varied by ±10% in the data. The total effect on the measured cross sections is smaller than 1% and considered negligible.

Positive and negative deviations with respect to the nominal values in each $p_{\rm T}^{\rm jet}$ bin are added separately in quadrature. Figure 7 shows the total systematic uncertainty as a function of $p_{\rm T}^{\rm jet}$ in the different $|y^{\rm jet}|$ regions, where an additional 5.8% uncertainty on the total luminosity is not included.

XI. QCD PREDICTIONS

The measurements are compared to parton-level NLO pQCD predictions, as computed using JETRAD [10] with CTEQ6.1M PDFs [11] and the renormalization and factorization scales (μ_R and μ_F) both set to $\mu_0 = max(p_{\rm T}^{\rm jet})/2$. Different sources of uncertainty on the theoretical predictions are considered. The main contribution comes from the uncertainty on the PDFs and is computed using the Hessian method [43]. At low $p_{\rm T}^{\rm jet}$, the uncertainty is about $\pm 5\%$ and approximately independent of $y^{\rm jet}$. The uncertainty increases as $p_{\rm T}^{\rm jet}$ and $|y^{\rm jet}|$ increase. At very high $p_{\rm T}^{\rm jet}$, the uncertainty varies between $^{+60\%}_{-30\%}$ and $^{+130\%}_{-40\%}$ for jets with $|y^{\rm jet}| < 0.1$ and $1.6 < |y^{\rm jet}| < 2.1$, respectively, and is dominated by the limited knowledge of the gluon PDF. An increase of μ_R and μ_F from μ_0 to $2\mu_0$ changes the theoretical predictions by only a few percent. Values significantly smaller than μ_0 lead to unstable NLO results and are not considered.

The theoretical predictions include a correction factor, $\mathrm{C_{HAD}}(p_{\rm T}^{\rm jet}, y^{\rm jet})$, that approximately accounts for non-perturbative contributions from the underlying event and fragmentation of partons into hadrons (see Fig. 8 and Tables IV-V). In each jet rapidity region, $\mathrm{C_{HAD}}$ is estimated, using PYTHIA-TUNE A, as the ratio between the nominal $p_{\rm T,had}^{\rm jet}$ distribution and the one obtained after removing the interactions between p and $\overline{p}$ remnants and the fragmentation into hadrons in the Monte Carlo samples. The correction decreases as $p_{\rm T}^{\rm jet}$ increases and shows a moderate $|y^{\rm jet}|$ dependence. At low $p_{\rm T}^{\rm jet}$, $\mathrm{C_{HAD}}$ varies between 1.18 and 1.13 as $|y^{\rm jet}|$ increases, and it becomes of the order of 1.02 at very high $p_{\rm T}^{\rm jet}$. The uncertainty on $\mathrm{C_{HAD}}$ varies between $\pm 9\%$ and $\pm 12\%$ at low $p_{\rm T}^{\rm jet}$ and decreases to about $\pm 1\%$ at very high $p_{\rm T}^{\rm jet}$, as determined from the difference between the parton-to-hadron correction factors obtained using HERWIG instead of PYTHIA-TUNE A.

XII. RESULTS

The measured inclusive jet cross sections, $d^2\sigma/dp_{\rm T}^{\rm jet}dy^{\rm jet}$, refer to hadron-level jets, reconstructed using the $k_{\rm T}$ algorithm with $D = 0.7$, in the region $p_{\rm T}^{\rm jet} > 54$ GeV/c and $|y^{\rm jet}| < 2.1$. Figure 9 shows the measured cross sections as a function of $p_{\rm T}^{\rm jet}$ in five different $|y^{\rm jet}|$ regions compared to NLO pQCD predictions. The data are reported in Tables IV-V. The measured cross sections decrease by more than seven to eight orders of magnitude as $p_{\rm T}^{\rm jet}$ increases. Figure 10 shows the ratio data/theory as a function of $p_{\rm T}^{\rm jet}$ in the five different $|y^{\rm jet}|$ regions. Good agreement is observed in the whole range in $p_{\rm T}^{\rm jet}$ and $y^{\rm jet}$ between the measured cross sections and the theoretical predictions. In particular, no significant deviation from the pQCD prediction is observed for central jets at high $p_{\rm T}^{\rm jet}$. The corresponding χ^2 tests, relative to the nominal pQCD prediction and performed separately in each $|y^{\rm jet}|$ region, give probabilities that vary between 9% and 90%. A global χ^2 test, applied to all the data points in all $|y^{\rm jet}|$ regions simultaneously, gives a probability of 7%. In both cases, a detailed treatment of correlations between systematic uncertainties was considered, as discussed in Appendix A. In addition, Fig. 10 shows the ratio of pQCD predictions using MRST2004 [12] and CTEQ6.1M PDF sets, well inside the theoretical and experimental uncertainties. The uncertainty on the measured cross sections at high $p_{\rm T}^{\rm jet}$, compared to that on the theoretical predictions, indicates that the data presented in this article will contribute to a better understanding of the gluon PDF.

Finally, in the region $0.1 < |y^{\rm jet}| < 0.7$, the analysis is repeated using different values for D in the $k_{\rm T}$ algorithm: $D = 0.5$ and $D = 1.0$. In both cases, good agreement is observed between the measured cross sections and the NLO pQCD predictions in the whole range in $p_{\rm T}^{\rm jet}$ (see Fig. 11 and Tables VI-VII). The corresponding χ^2 tests give probabilities of 84% and 22% for $D = 0.5$ and $D = 1.0$, respectively. As D decreases, the measurement is less sensitive to contributions from multiple $p\overline{p}$ interactions per bunch crossing, and the presence and proper modeling of the underlying event. For $D = 0.5$ ($D = 1.0$), the value for $\delta_{p_{\rm T}}^{\rm mi}$ becomes 1.18 ± 0.12 (3.31 ± 0.47) GeV/c, and the parton-to-hadron correction factor applied to the pQCD predictions is $\mathrm{C_{HAD}} = 1.1$ ($\mathrm{C_{HAD}} = 1.4$) at low $p_{\rm T}^{\rm jet}$.

XIII. SUMMARY AND CONCLUSIONS

We have presented results on inclusive jet production in $p\overline{p}$ collisions at $\sqrt{s} = 1.96$ TeV for jets with transverse momentum $p_{\rm T}^{\rm jet} > 54$ GeV/c and rapidity in the region $|y^{\rm jet}| < 2.1$, using the $k_{\rm T}$ algorithm and based on 1.0 fb^{-1} of CDF Run II data. The measured cross sections are in agreement with NLO pQCD predictions after the necessary non-perturbative parton-to-hadron corrections are taken into account. The results reported in this article should contribute to a better understanding of the gluon PDF inside the proton when used in QCD global fits.

Acknowledgments

We thank the Fermilab staff and the technical staffs of the participating institutions for their vital contributions. This work was supported by the U.S. Department of Energy and National Science Foundation; the Italian Istituto Nazionale di Fisica Nucleare; the Ministry of Education, Culture, Sports, Science and Technology of Japan; the Natural Sciences and Engineering Research Council of Canada; the National Science Council of the Republic of China; the Swiss National Science Foundation; the A.P. Sloan Foundation; the Bundesministerium für Bildung und Forschung, Germany; the Korean Science and Engineering Foundation and the Korean Research Foundation; the Particle Physics and Astronomy Research Council and the Royal Society, UK; the Institut National de Physique Nucleaire et Physique des Particules/CNRS; the Russian Foundation for Basic Research; the Comisión Interministerial de Ciencia y Tecnología, Spain; the European Community's Human Potential Programme under contract HPRN-CT-2002-00292; and the Academy of Finland.

[1] D.J. Gross and F. Wilczek, Phys. Rev. D **8**, 3633 (1973);
H. Fritzsch, M. Gell-Mann, H. Leutwyler, Phys. Lett. **B47**, 365 (1973).
[2] A. Abulencia *et al.* (CDF Collaboration), Phys. Rev. Lett. **96**, 122001 (2006).
[3] A. Abulencia *et al.* (CDF Collaboration), Phys. Rev. D **74**, 071103(R) (2006).
[4] T. Affolder *et al.* (CDF Collaboration), Phys. Rev. D **64**, 032001 (2001). [Erratum-ibid. D **65**, 039903 (2002)].
[5] B. Abbott *et al.* (DØ Collaboration), Phys. Rev. Lett. **82**, 2451 (1999).
[6] V.M. Abazov *et al.* (DØ Collaboration), Phys. Lett. B **525**, 211 (2002).
[7] S. Catani *et al.*, Nucl. Phys. **B406**, 187 (1993).
[8] S.D. Ellis and D.E. Soper, Phys. Rev. D **48**, 3160 (1993).
[9] We use a cylindrical coordinate system about the beam axis in which the proton defines the positive z-direction, θ is the polar angle, and ϕ is the azimuthal angle. We define $E_T = E\ sin\theta$, $p_T = p\ sin\theta$, $\eta = -ln(tan(\frac{\theta}{2}))$, and $y = \frac{1}{2}ln(\frac{E+p_z}{E-p_z})$.
[10] W.T. Giele, E.W.N. Glover, D.A. Kosower, Nucl. Phys. **B403**, 633 (1993).
[11] J. Pumplin *et al.*, J. High Energy Phys. **0207**, 012 (2002).
[12] A.D. Martin *et al.*, Eur. Phys. J. C **23**, 73 (2002).
[13] The hadron level in the Monte Carlo generators is defined using all final-state particles with lifetime above $10^{-11}s$.
[14] D. Acosta *et al.* (CDF Collaboration), Phys. Rev. D **71**, 032001 (2005).
[15] A. Sill *et al.*, Nucl. Instrum. Methods A **447**, 1 (2000);
A. Affolder *et al.*, Nucl. Instrum. Methods A **453**, 84 (2000);
C.S. Hill, Nucl. Instrum. Methods A **530**, 1 (2000).
[16] T. Affolder *et al.*, Nucl. Instrum. Methods A **526**, 249 (2004).
[17] L. Balka *et al.*, Nucl. Instrum. Methods A **267**, 272 (1988);
S.R. Hahn, *et al.*, Nucl. Instrum. Methods A **267** 351 (1988).
[18] S. Bertolucci *et al.*, Nucl. Instrum. Methods A **267**, 301 (1988).
[19] R. Oishi, Nucl. Instrum. Methods A **453**, 277 (2000);
M.G. Albrow *et al.*, Nucl. Instrum. Methods A **480**, 524 (2002).
[20] D. Acosta *et al.*, Nucl. Instrum. Meth., A **494**, 57 (2002).
[21] The electromagnetic and hadronic sections of a calorimeter tower are defined massless. For each of them, the four-momentum is constructed using its energy and its position with respect to the interaction point.
[22] B.L. Winer, Int. J. Mod. Phys. A **16S1C**, 1169 (2001).
[23] In order to reduce online trigger rates, different prescale factors are applied to trigger paths. For a given trigger path, a prescale of 1000 would indicate that only one of every 1000 events satisfying the trigger requirements is selected.
[24] A trigger tower is defined adding the information of two adjacent calorimeter towers.
[25] F. Abe *et al.* (CDF Collaboration), Phys. Rev. D **45**, 1448 (1992).
[26] $\not\!\!E_T$ is defined as the norm of $-\sum_i E_T^i \cdot \vec{n}_i$, where $\vec{n}_i$ is the unit vector in the azimuthal plane that points from the beamline to the i-th calorimeter tower.
[27] R. Brun *et al.*, Tech. Rep. CERN-DD/EE/84-1, 1987 (unpublished).

[28] G. Grindhammer, M. Rudowicz and S. Peters, Nucl. Instrum. Methods A **290**, 469 (1990).
[29] T. Sjöstrand *et al.*, Comp. Phys. Comm. **135**, 238 (2001).
[30] G. Corcella *et al.*, J. High Energy Phys. **0101**, 010 (2001).
[31] H.L. Lai *et al.*, Eur. Phys. J. C **12**, 375 (2000).
[32] PYTHIA-TUNE A Monte Carlo samples are generated using the following tuned parameters in PYTHIA: PARP(67) = 4.0, MSTP(82) = 4, PARP(82) = 2.0, PARP(84) = 0.4, PARP(85) = 0.9, PARP(86) = 0.95, PARP(89) = 1800.0, PARP(90) = 0.25.
[33] T. Affolder *et al.* (CDF Collaboration), Phys. Rev. D **65**, 092002 (2002).
[34] D. Acosta *et al.* (CDF Collaboration), Phys. Rev. D **71**, 112002 (2005).
[35] B. Andersson *et al.*, Phys. Rep. **97**, 31 (1983).
[36] T. Sjöstrand, Comp. Phys. Comm. **39**, 347 (1986).
[37] B.R. Webber, Nucl. Phys. **B238**, 492 (1984).
[38] P. Bagnaia *et al.* (UA2 Collaboration), Phys. Lett. B **144**, 283 (1984).
[39] If considered event-by-event, β is equivalent to $p_{\mathrm{T,cal}}^{\text{test jet}}/p_{\mathrm{T,cal}}^{\text{ref. jet}}$. However, Eq. (2) is preferred since Δ follows a Gaussian distribution while the ratio $p_{\mathrm{T,cal}}^{\text{test jet}}/p_{\mathrm{T,cal}}^{\text{ref. jet}}$ suffers from important non-Gaussian tails.
[40] $\hat{p}_t$ is defined for two-body reactions in terms of Mandelstam variables as $\hat{p}_t = \sqrt{\frac{\hat{t}\cdot\hat{u}}{\hat{s}}}$.
[41] O. Norniella, *Inclusive Jet Production Studies at the Tevatron using the CDF Detector*, Ph.D. thesis, Universidad Autónoma de Barcelona, 2007.
[42] A. Bhatti *et al.*, Nucl. Instrum. Methods A **566**, 375 (2006).
[43] J. Pumplin *et al.*, Phys. Rev. D **65**, 014013 (2002).

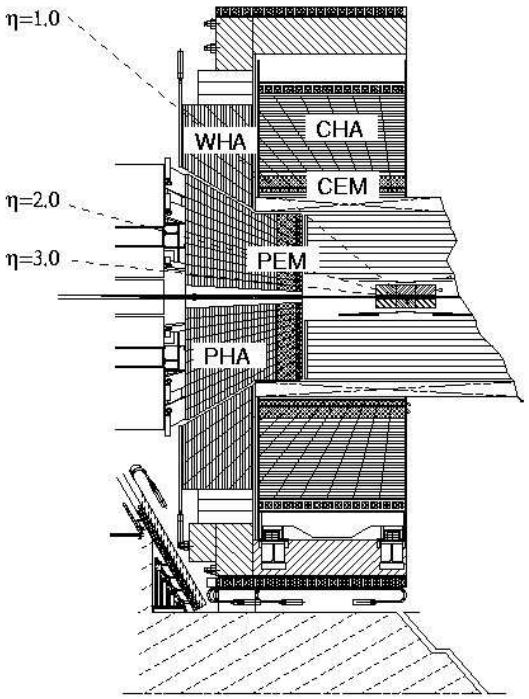

FIG. 1: Elevation view of one half of the CDF detector displaying the components of the CDF calorimeter.

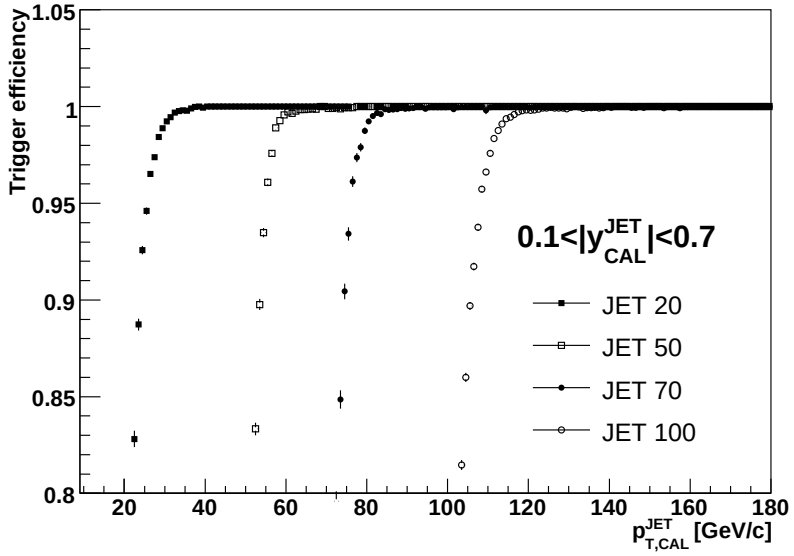

FIG. 2: Measured trigger efficiencies as a function of $p_{\mathrm{T,cal}}^{\mathrm{jet}}$ for different trigger paths and in the region $0.1 < |y_{\mathrm{cal}}^{\mathrm{jet}}| < 0.7$.

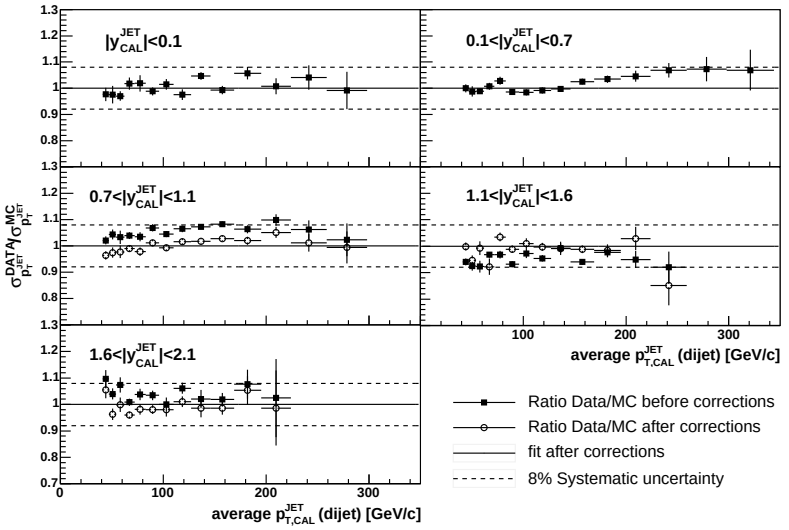

FIG. 3: Ratio $\sigma^{\rm data}_{p_{\rm T}^{\rm jet}}/\sigma^{\rm mc}_{p_{\rm T}^{\rm jet}}$ as a function of the average $p^{\rm jet}_{\rm T,cal}$ of the dijet event, in different $|y^{\rm jet}_{\rm cal}|$ regions, before (black squares) and after (open circles) corrections have been applied (see Section VII). The solid lines are fits to the corrected ratios. The dashed lines indicate a $\pm 8\%$ relative variation considered in the study of systematic uncertainties.

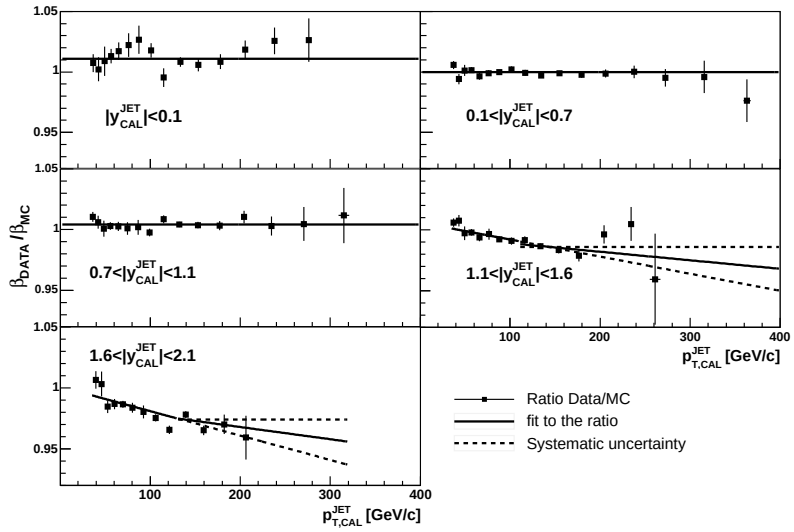

FIG. 4: Ratio $\beta_{\rm data}/\beta_{\rm mc}$ as a function of $p^{\rm jet}_{\rm T,cal}$ in different $|y^{\rm jet}_{\rm cal}|$ regions. The solid lines show the nominal parameterizations based on fits to the ratios. In the region $|y^{\rm jet}_{\rm cal}| > 1.1$, the dashed lines indicate different parameterizations used to describe the ratios at high $p^{\rm jet}_{\rm T,cal}$, and are considered in the study of systematic uncertainties.

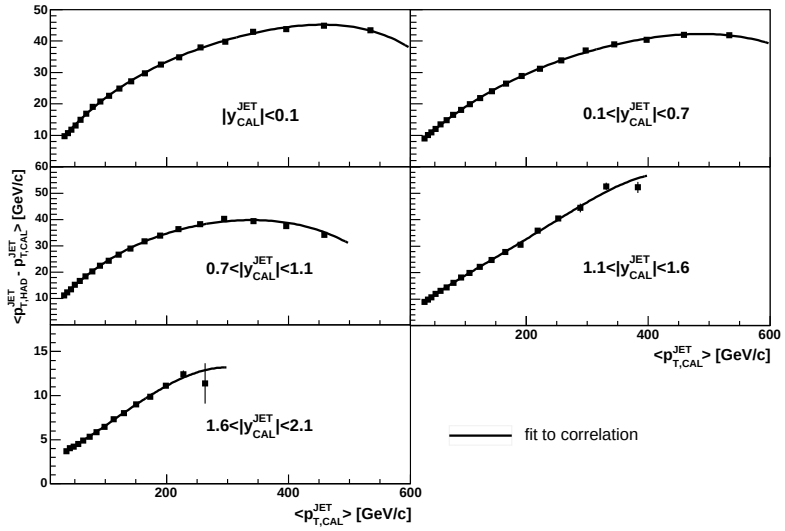

FIG. 5: Correlation $\langle p_{\mathrm{T,had}}^{\mathrm{jet}} - p_{\mathrm{T,cal}}^{\mathrm{jet}} \rangle$ versus $\langle p_{\mathrm{T,cal}}^{\mathrm{jet}} \rangle$, as extracted from PYTHIA TUNE A simulated event samples, in the different $|y_{\mathrm{cal}}^{\mathrm{jet}}|$ regions.

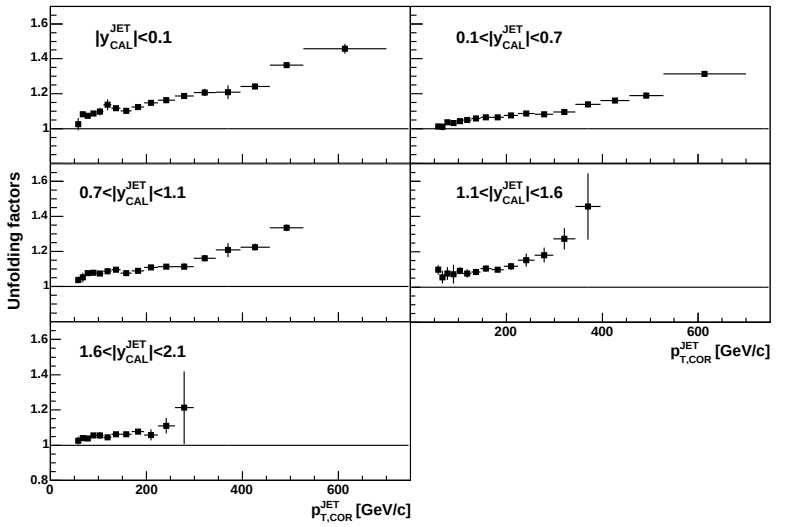

FIG. 6: Unfolding factors, $U(p_{\mathrm{T,cor}}^{\mathrm{jet}}, y_{\mathrm{cal}}^{\mathrm{jet}})$, as extracted from PYTHIA TUNE A simulated event samples, as a function of $p_{\mathrm{T,cor}}^{\mathrm{jet}}$ in the different $|y_{\mathrm{cal}}^{\mathrm{jet}}|$ regions.

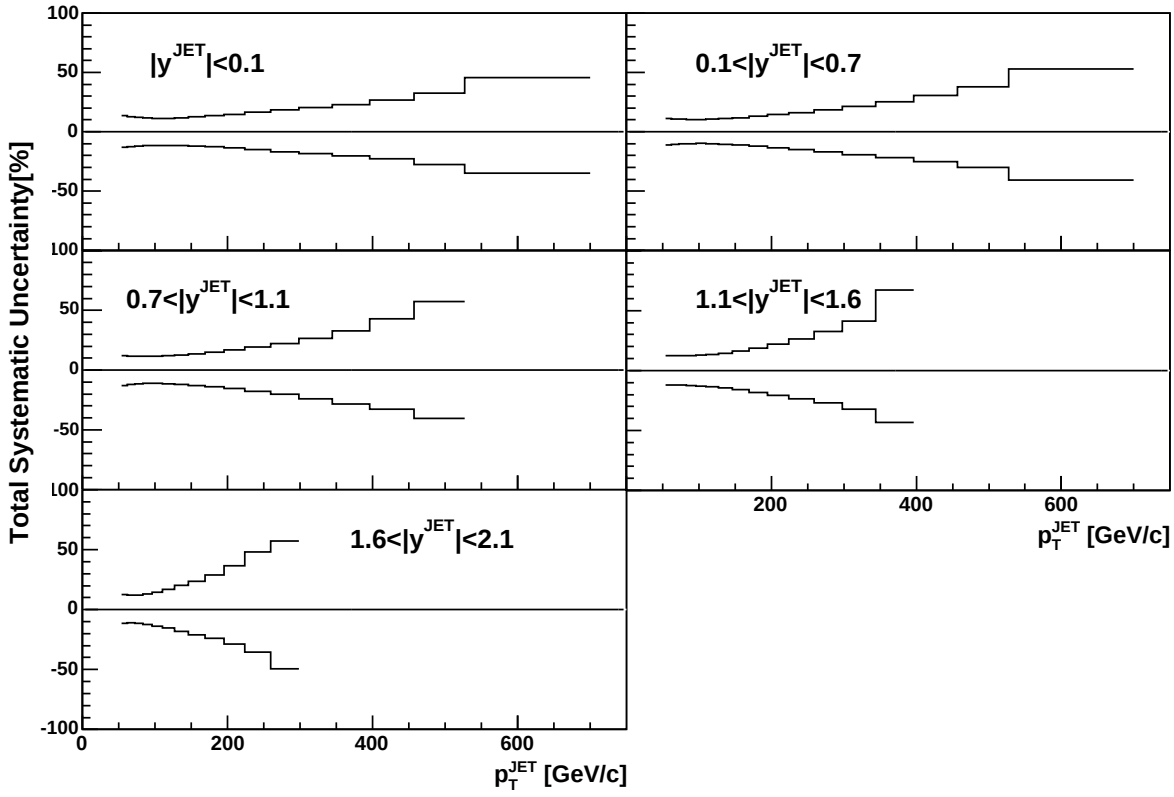

FIG. 7: Total systematic uncertainty (in percent) on the measured inclusive differential jet cross sections as a function $p_{\mathrm{T}}^{\mathrm{jet}}$ for the different $|y^{\mathrm{jet}}|$ regions (see Tables II-III). An additional 5.8% uncertainty on the integrated luminosity is not included.

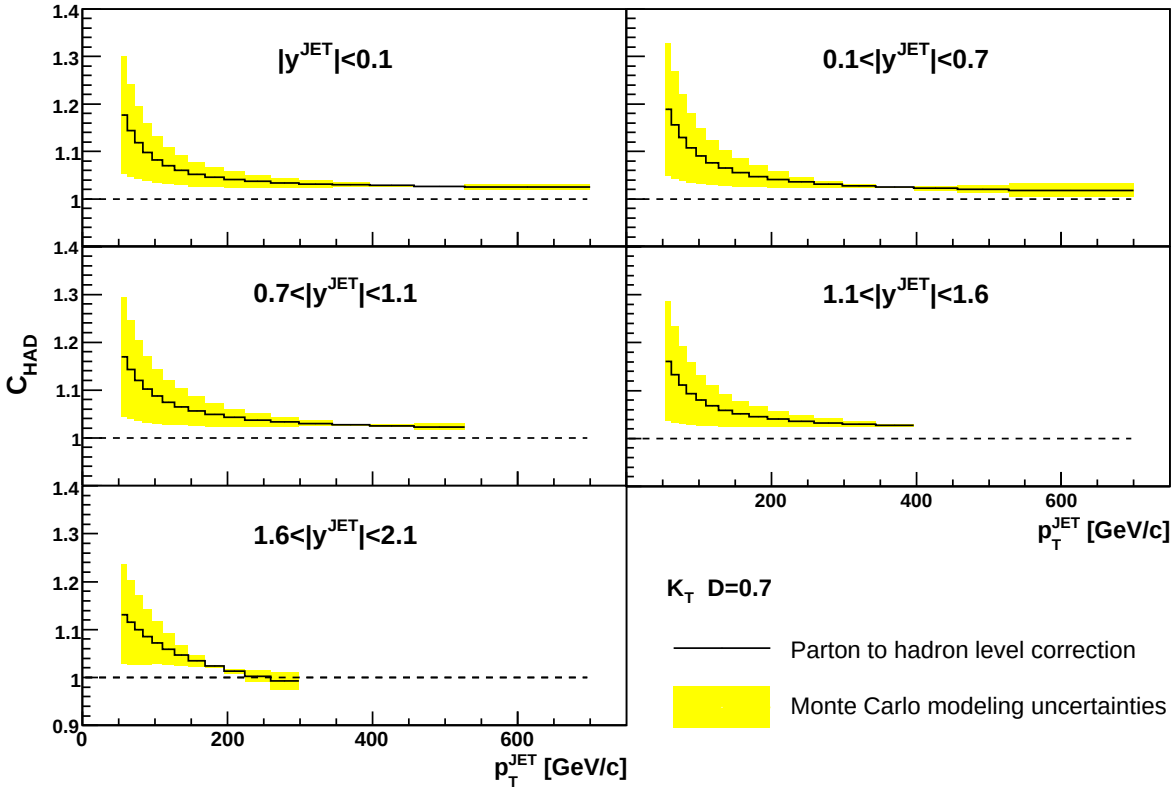

FIG. 8: Magnitude of the parton-to-hadron correction, $C_{HAD}(p_T^{jet}, y^{jet})$, used to correct the NLO pQCD predictions (see Tables IV-V). The shaded bands indicate the quoted Monte Carlo modeling uncertainty.

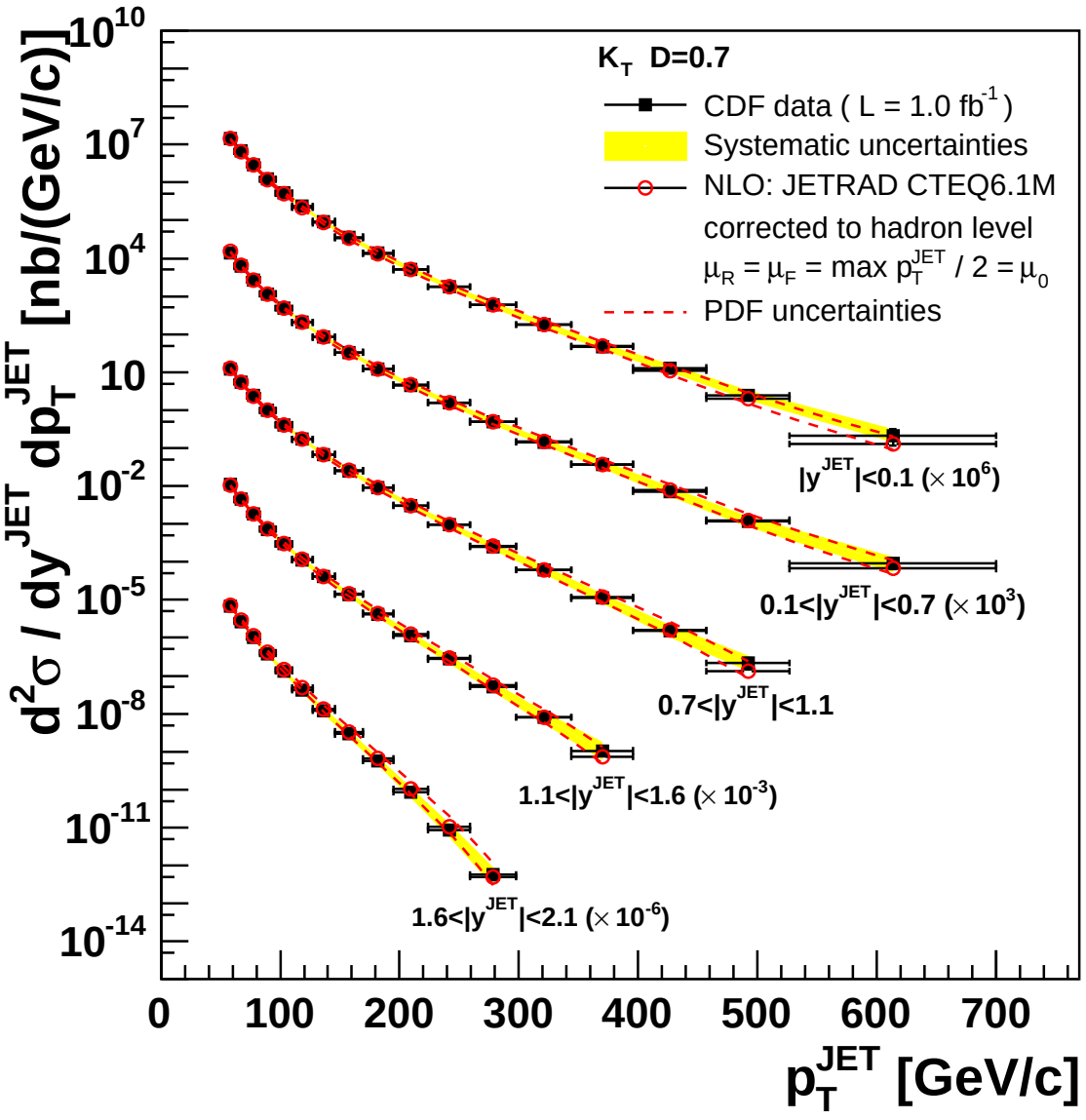

FIG. 9: Measured inclusive differential jet cross sections (black squares) as a function of $p_{\mathrm{T}}^{\mathrm{jet}}$ for jets with $p_{\mathrm{T}}^{\mathrm{jet}} > 54$ GeV/c in different $|y^{\mathrm{jet}}|$ regions compared to NLO pQCD predictions (open circles). The shaded bands show the systematic uncertainty on the measurements (see Tables IV-V). A 5.8% uncertainty on the integrated luminosity is not included. The dashed lines indicate the PDF uncertainty on the theoretical predictions. For presentation, the measurements in different $|y^{\mathrm{jet}}|$ regions are scaled by different global factors. Factors ($\times 10^6$), ($\times 10^3$), ($\times 10^{-3}$), and ($\times 10^{-6}$) are used in the regions $|y^{\mathrm{jet}}| < 0.1$, $0.1 < |y^{\mathrm{jet}}| < 0.7$, $1.1 < |y^{\mathrm{jet}}| < 1.6$, and $1.6 < |y^{\mathrm{jet}}| < 2.1$, respectively.

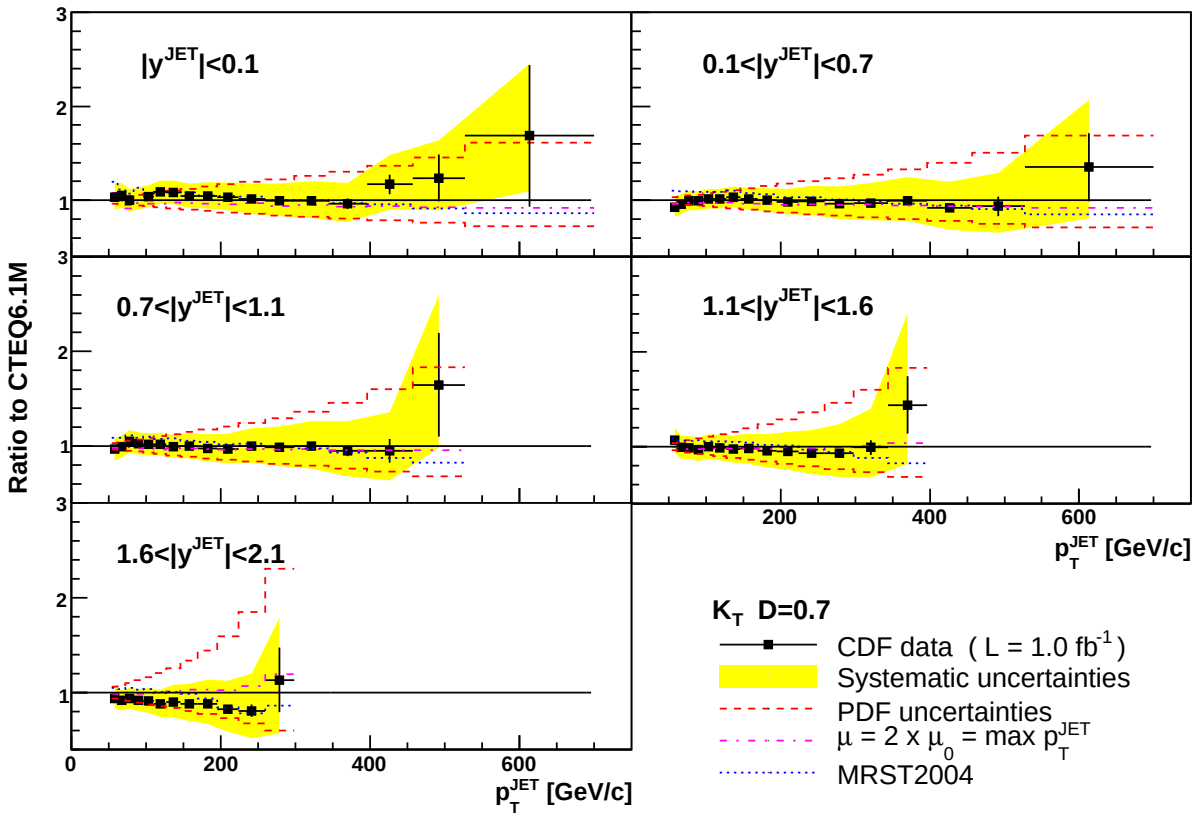

FIG. 10: Ratio data/theory as a function of $p_{\mathrm{T}}^{\mathrm{jet}}$ in different $|y^{\mathrm{jet}}|$ regions. The error bars (shaded bands) show the total statistical (systematic) uncertainty on the data. A 5.8% uncertainty on the integrated luminosity is not included. The dashed lines indicate the PDF uncertainty on the theoretical predictions. The dotted lines present the ratio of NLO pQCD predictions using MRST2004 and CTEQ6.1M PDFs. The dotted-dashed lines show the ratios of pQCD predictions with $2\mu_0$ and μ_0.

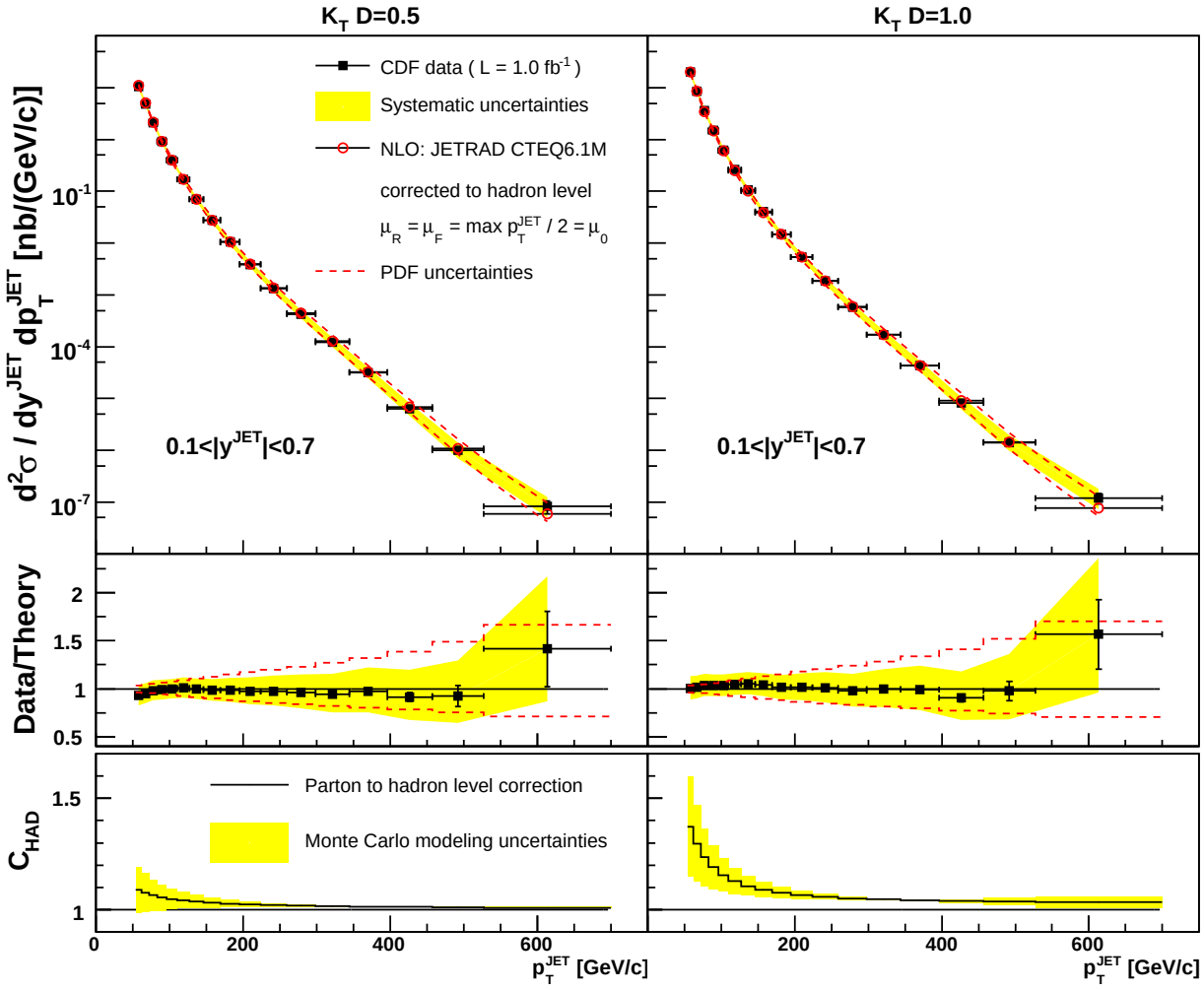

FIG. 11: (top) Measured inclusive differential jet cross sections (black squares) as a function of $p_{\mathrm{T}}^{\mathrm{jet}}$ for jets with $p_{\mathrm{T}}^{\mathrm{jet}} > 54$ GeV/c and $0.1 < |y^{\mathrm{jet}}| < 0.7$ using the k_{T} parameter $D = 0.5$ (left) and $D = 1.0$ (right), compared to NLO pQCD predictions (open circles). The shaded bands show the total systematic uncertainty on the measurements (see Tables VI-VII). A 5.8% uncertainty on the integrated luminosity is not included. The dashed lines indicate the PDF uncertainty on the theoretical predictions. (middle) Ratio data/theory as a function of $p_{\mathrm{T}}^{\mathrm{jet}}$ for $D = 0.5$ (left) and $D = 1.0$ (right). (bottom) Magnitude of the parton-to-hadron corrections, $\mathrm{C_{HAD}}(p_{\mathrm{T}}^{\mathrm{jet}})$, used to correct the NLO pQCD predictions for $D = 0.5$ (left) and $D = 1.0$ (right). The shaded bands indicate the quoted Monte Carlo modeling uncertainty.

Systematic uncertainties [%] ($\|y^{\rm jet}\| < 0.1$)								
$p_{\rm T}^{\rm jet}$ [GeV/c]	jet energy scale	$\beta_{\rm data}/\beta_{\rm mc}$ (a)	(b)	(c)	resolution	unfolding	$p_{\rm T}^{\rm jet}$-spectra	$\delta_{p_{\rm T}}^{\rm mi}$
54 - 62	$^{+10.3}_{-9.3}$	$^{+1.4}_{-2.1}$	–	–	$^{+2.8}_{-3.0}$	±8.2	±1.5	$^{+1.8}_{-1.7}$
62 - 72	$^{+9.9}_{-9.4}$	$^{+1.7}_{-2.1}$	–	–	$^{+2.8}_{-3.0}$	±7.1	±1.4	$^{+1.6}_{-1.5}$
72 - 83	$^{+9.6}_{-9.4}$	$^{+1.9}_{-2.1}$	–	–	$^{+2.9}_{-3.0}$	±6.2	±1.3	$^{+1.4}_{-1.3}$
83 - 96	$^{+9.4}_{-9.5}$	$^{+2.1}_{-2.2}$	–	–	$^{+2.9}_{-2.9}$	±5.4	±1.1	$^{+1.3}_{-1.1}$
96 - 110	$^{+9.5}_{-9.6}$	$^{+2.3}_{-2.2}$	–	–	$^{+2.9}_{-2.9}$	±4.7	±1.0	$^{+1.1}_{-1.0}$
110 - 127	$^{+9.8}_{-9.8}$	$^{+2.5}_{-2.3}$	–	–	$^{+3.0}_{-2.9}$	±4.2	±0.9	$^{+1.0}_{-0.9}$
127 - 146	$^{+10.4}_{-10.2}$	$^{+2.7}_{-2.4}$	–	–	$^{+3.1}_{-2.9}$	±3.7	±0.8	$^{+0.9}_{-0.8}$
146 - 169	$^{+11.2}_{-10.8}$	$^{+2.8}_{-2.6}$	–	–	$^{+3.1}_{-3.0}$	±3.2	±0.6	$^{+0.8}_{-0.8}$
169 - 195	$^{+12.4}_{-11.6}$	$^{+2.9}_{-2.7}$	–	–	$^{+3.3}_{-3.0}$	±2.8	±0.5	$^{+0.7}_{-0.7}$
195 - 224	$^{+13.9}_{-12.8}$	$^{+3.0}_{-2.9}$	–	–	$^{+3.4}_{-3.2}$	±2.5	±0.4	$^{+0.6}_{-0.7}$
224 - 259	$^{+15.5}_{-14.3}$	$^{+3.1}_{-3.1}$	–	–	$^{+3.7}_{-3.4}$	±2.2	±0.3	$^{+0.6}_{-0.6}$
259 - 298	$^{+17.4}_{-15.9}$	$^{+3.3}_{-3.4}$	–	–	$^{+4.0}_{-3.6}$	±2.0	±0.4	$^{+0.5}_{-0.6}$
298 - 344	$^{+19.5}_{-17.4}$	$^{+3.6}_{-3.7}$	–	–	$^{+4.3}_{-4.0}$	±1.8	±0.6	$^{+0.5}_{-0.6}$
344 - 396	$^{+22.1}_{-19.1}$	$^{+4.0}_{-4.0}$	–	–	$^{+4.8}_{-4.5}$	±1.6	±1.0	$^{+0.4}_{-0.5}$
396 - 457	$^{+25.7}_{-21.6}$	$^{+4.6}_{-4.4}$	–	–	$^{+5.4}_{-5.1}$	±1.4	±1.8	$^{+0.4}_{-0.5}$
457 - 527	$^{+31.3}_{-26.3}$	$^{+5.3}_{-5.1}$	–	–	$^{+6.1}_{-5.9}$	±1.3	±3.1	$^{+0.3}_{-0.5}$
527 - 700	$^{+43.7}_{-32.9}$	$^{+7.3}_{-6.7}$	–	–	$^{+7.4}_{-7.3}$	±1.1	±7.1	$^{+0.3}_{-0.5}$
Systematic uncertainties [%] ($0.1 < \|y^{\rm jet}\| < 0.7$)								
$p_{\rm T}^{\rm jet}$ [GeV/c]	jet energy scale	$\beta_{\rm data}/\beta_{\rm mc}$ (a)	(b)	(c)	resolution	unfolding	$p_{\rm T}^{\rm jet}$-spectra	$\delta_{p_{\rm T}}^{\rm mi}$
54 - 62	$^{+9.5}_{-9.4}$	–	–	–	$^{+2.2}_{-2.5}$	±5.3	±0.6	$^{+1.6}_{-1.6}$
62 - 72	$^{+9.4}_{-9.1}$	–	–	–	$^{+2.1}_{-2.4}$	±4.7	±0.6	$^{+1.5}_{-1.4}$
72 - 83	$^{+9.4}_{-8.9}$	–	–	–	$^{+2.1}_{-2.4}$	±4.1	±0.5	$^{+1.3}_{-1.3}$
83 - 96	$^{+9.4}_{-8.9}$	–	–	–	$^{+2.0}_{-2.3}$	±3.7	±0.5	$^{+1.2}_{-1.1}$
96 - 110	$^{+9.6}_{-9.0}$	–	–	–	$^{+2.0}_{-2.2}$	±3.3	±0.5	$^{+1.1}_{-1.0}$
110 - 127	$^{+10.0}_{-9.3}$	–	–	–	$^{+1.9}_{-2.1}$	±3.0	±0.5	$^{+1.0}_{-0.9}$
127 - 146	$^{+10.6}_{-9.8}$	–	–	–	$^{+1.9}_{-2.1}$	±2.7	±0.5	$^{+0.9}_{-0.8}$
146 - 169	$^{+11.4}_{-10.6}$	–	–	–	$^{+1.9}_{-2.0}$	±2.4	±0.4	$^{+0.8}_{-0.8}$
169 - 195	$^{+12.6}_{-11.7}$	–	–	–	$^{+2.0}_{-2.1}$	±2.2	±0.4	$^{+0.7}_{-0.7}$
195 - 224	$^{+14.1}_{-13.1}$	–	–	–	$^{+2.1}_{-2.1}$	±2.0	±0.4	$^{+0.7}_{-0.7}$
224 - 259	$^{+16.0}_{-14.8}$	–	–	–	$^{+2.2}_{-2.3}$	±1.8	±0.3	$^{+0.6}_{-0.6}$
259 - 298	$^{+18.4}_{-16.7}$	–	–	–	$^{+2.5}_{-2.5}$	±1.7	±0.3	$^{+0.6}_{-0.6}$
298 - 344	$^{+21.3}_{-18.9}$	–	–	–	$^{+2.8}_{-2.9}$	±1.6	±0.3	$^{+0.5}_{-0.6}$
344 - 396	$^{+25.1}_{-21.4}$	–	–	–	$^{+3.4}_{-3.5}$	±1.5	±0.5	$^{+0.5}_{-0.5}$
396 - 457	$^{+30.3}_{-24.7}$	–	–	–	$^{+4.1}_{-4.2}$	±1.4	±0.8	$^{+0.4}_{-0.5}$
457 - 527	$^{+37.7}_{-29.3}$	–	–	–	$^{+5.1}_{-5.2}$	±1.3	±1.4	$^{+0.4}_{-0.5}$
527 - 700	$^{+52.3}_{-39.8}$	–	–	–	$^{+7.3}_{-7.3}$	±1.2	±3.6	$^{+0.4}_{-0.5}$

TABLE II: Systematic uncertainties (in percent) on the measured inclusive jet differential cross section as a function of $p_{\rm T}^{\rm jet}$ for jets in the regions $|y^{\rm jet}| < 0.1$ and $0.1 < |y^{\rm jet}| < 0.7$ (see Fig. 7). The different columns follow the discussion in Section X. An additional 5.8% uncertainty on the integrated luminosity is not included.

Systematic uncertainties [%] ($0.7 < \|y^{\rm jet}\| < 1.1$)								
$p_{\rm T}^{\rm jet}$ [GeV/c]	jet energy scale	$\beta_{\rm data}/\beta_{\rm mc}$ (a)	(b)	(c)	resolution	unfolding	$p_{\rm T}^{\rm jet}$-spectra	$\delta_{p_{\rm T}}^{\rm mi}$
54 - 62	$^{+9.2}_{-9.9}$	$^{+2.1}_{-2.3}$	–	–	$^{+4.0}_{-3.8}$	±6.3	±2.0	$^{+1.7}_{-1.6}$
62 - 72	$^{+9.2}_{-9.3}$	$^{+2.2}_{-2.3}$	–	–	$^{+3.8}_{-3.7}$	±5.6	±1.9	$^{+1.5}_{-1.4}$
72 - 83	$^{+9.2}_{-9.0}$	$^{+2.3}_{-2.3}$	–	–	$^{+3.7}_{-3.5}$	±4.9	±1.8	$^{+1.3}_{-1.3}$
83 - 96	$^{+9.5}_{-9.0}$	$^{+2.3}_{-2.3}$	–	–	$^{+3.5}_{-3.4}$	±4.4	±1.8	$^{+1.2}_{-1.2}$
96 - 110	$^{+9.9}_{-9.3}$	$^{+2.4}_{-2.4}$	–	–	$^{+3.4}_{-3.3}$	±3.9	±1.7	$^{+1.1}_{-1.1}$
110 - 127	$^{+10.6}_{-9.8}$	$^{+2.5}_{-2.5}$	–	–	$^{+3.3}_{-3.2}$	±3.5	±1.7	$^{+1.0}_{-1.0}$
127 - 146	$^{+11.5}_{-10.7}$	$^{+2.6}_{-2.6}$	–	–	$^{+3.3}_{-3.1}$	±3.2	±1.7	$^{+0.9}_{-0.9}$
146 - 169	$^{+12.6}_{-11.7}$	$^{+2.8}_{-2.7}$	–	–	$^{+3.3}_{-3.2}$	±2.8	±1.6	$^{+0.8}_{-0.8}$
169 - 195	$^{+14.1}_{-13.0}$	$^{+3.0}_{-2.9}$	–	–	$^{+3.4}_{-3.3}$	±2.6	±1.6	$^{+0.8}_{-0.8}$
195 - 224	$^{+15.9}_{-14.6}$	$^{+3.3}_{-3.2}$	–	–	$^{+3.7}_{-3.5}$	±2.3	±1.7	$^{+0.7}_{-0.7}$
224 - 259	$^{+18.1}_{-16.5}$	$^{+3.8}_{-3.6}$	–	–	$^{+4.1}_{-3.9}$	±2.1	±1.8	$^{+0.7}_{-0.7}$
259 - 298	$^{+21.0}_{-19.2}$	$^{+4.4}_{-4.1}$	–	–	$^{+4.7}_{-4.5}$	±2.0	±2.1	$^{+0.6}_{-0.6}$
298 - 344	$^{+25.2}_{-22.7}$	$^{+5.0}_{-4.8}$	–	–	$^{+5.6}_{-5.3}$	±1.8	±2.4	$^{+0.6}_{-0.6}$
344 - 396	$^{+31.5}_{-26.9}$	$^{+5.9}_{-5.6}$	–	–	$^{+6.8}_{-6.4}$	±1.7	±3.0	$^{+0.6}_{-0.6}$
396 - 457	$^{+41.3}_{-31.0}$	$^{+7.2}_{-6.6}$	–	–	$^{+8.3}_{-7.7}$	±1.6	±3.8	$^{+0.5}_{-0.5}$
457 - 527	$^{+55.4}_{-38.3}$	$^{+10.4}_{-7.7}$	–	–	$^{+10.0}_{-9.1}$	±1.5	±5.0	$^{+0.5}_{-0.5}$
Systematic uncertainties [%] ($1.1 < \|y^{\rm jet}\| < 1.6$)								
$p_{\rm T}^{\rm jet}$ [GeV/c]	jet energy scale	$\beta_{\rm data}/\beta_{\rm mc}$ (a)	(b)	(c)	resolution	unfolding	$p_{\rm T}^{\rm jet}$-spectra	$\delta_{p_{\rm T}}^{\rm mi}$
54 - 62	$^{+9.4}_{-8.6}$	$^{+2.6}_{-2.4}$	–	$^{+0.0}_{-3.0}$	$^{+2.9}_{-3.1}$	±6.7	±1.3	$^{+1.8}_{-1.8}$
62 - 72	$^{+9.5}_{-8.9}$	$^{+2.5}_{-2.4}$	–	$^{+0.0}_{-3.0}$	$^{+2.9}_{-3.0}$	±6.4	±1.1	$^{+1.6}_{-1.5}$
72 - 83	$^{+9.8}_{-9.3}$	$^{+2.5}_{-2.5}$	–	$^{+0.0}_{-3.0}$	$^{+2.9}_{-2.9}$	±6.1	±0.9	$^{+1.4}_{-1.3}$
83 - 96	$^{+10.2}_{-9.8}$	$^{+2.5}_{-2.6}$	–	$^{+0.0}_{-3.0}$	$^{+2.9}_{-2.8}$	±5.8	±0.8	$^{+1.3}_{-1.2}$
96 - 110	$^{+10.9}_{-10.5}$	$^{+2.6}_{-2.6}$	–	$^{+0.0}_{-3.0}$	$^{+3.0}_{-2.9}$	±5.6	±0.6	$^{+1.2}_{-1.1}$
110 - 127	$^{+11.7}_{-11.4}$	$^{+2.7}_{-2.8}$	–	$^{+0.0}_{-3.0}$	$^{+3.1}_{-3.0}$	±5.4	±0.4	$^{+1.1}_{-1.0}$
127 - 146	$^{+12.8}_{-12.6}$	$^{+2.9}_{-3.0}$	–	$^{+0.0}_{-3.0}$	$^{+3.4}_{-3.2}$	±5.2	±0.3	$^{+1.1}_{-1.0}$
146 - 169	$^{+14.5}_{-14.2}$	$^{+3.3}_{-3.3}$	–	$^{+0.0}_{-3.0}$	$^{+3.8}_{-3.6}$	±5.0	±0.1	$^{+1.0}_{-0.9}$
169 - 195	$^{+16.9}_{-16.2}$	$^{+3.8}_{-3.7}$	–	$^{+0.0}_{-3.0}$	$^{+4.3}_{-4.2}$	±4.8	±0.1	$^{+1.0}_{-0.9}$
195 - 224	$^{+20.3}_{-18.6}$	$^{+4.4}_{-4.2}$	$^{+0.7}_{-0.9}$	$^{+0.0}_{-3.0}$	$^{+5.1}_{-5.0}$	±4.7	±0.2	$^{+0.9}_{-0.9}$
224 - 259	$^{+24.7}_{-21.2}$	$^{+5.2}_{-5.0}$	$^{+2.6}_{-2.4}$	$^{+0.0}_{-3.0}$	$^{+6.2}_{-6.1}$	±4.6	±0.4	$^{+0.9}_{-0.9}$
259 - 298	$^{+29.9}_{-24.1}$	$^{+6.2}_{-5.9}$	$^{+6.3}_{-4.5}$	$^{+0.0}_{-3.0}$	$^{+7.8}_{-7.3}$	±4.4	±0.8	$^{+0.9}_{-0.9}$
298 - 344	$^{+37.2}_{-28.6}$	$^{+7.3}_{-7.1}$	$^{+12.6}_{-7.5}$	$^{+0.0}_{-3.0}$	$^{+9.8}_{-8.5}$	±4.3	±1.6	$^{+0.9}_{-0.9}$
344 - 396	$^{+61.2}_{-39.2}$	$^{+8.7}_{-8.3}$	$^{+22.7}_{-11.7}$	$^{+0.0}_{-3.0}$	$^{+12.4}_{-9.4}$	±4.2	±2.8	$^{+0.9}_{-0.9}$
Systematic uncertainties [%] ($1.6 < \|y^{\rm jet}\| < 2.1$)								
$p_{\rm T}^{\rm jet}$ [GeV/c]	jet energy scale	$\beta_{\rm data}/\beta_{\rm mc}$ (a)	(b)	(c)	resolution	unfolding	$p_{\rm T}^{\rm jet}$-spectra	$\delta_{p_{\rm T}}^{\rm mi}$
54 - 62	$^{+11.6}_{-10.3}$	$^{+2.3}_{-2.1}$	–	–	$^{+1.7}_{-1.6}$	±3.2	±1.0	$^{+2.1}_{-2.0}$
62 - 72	$^{+10.9}_{-10.1}$	$^{+2.4}_{-2.4}$	–	–	$^{+1.6}_{-1.7}$	±3.3	±0.8	$^{+1.8}_{-1.8}$
72 - 83	$^{+11.0}_{-10.3}$	$^{+2.6}_{-2.6}$	–	–	$^{+1.5}_{-1.7}$	±3.4	±0.6	$^{+1.7}_{-1.7}$
83 - 96	$^{+12.0}_{-11.1}$	$^{+2.8}_{-2.9}$	–	–	$^{+1.5}_{-1.8}$	±3.5	±0.4	$^{+1.6}_{-1.6}$
96 - 110	$^{+13.7}_{-12.5}$	$^{+3.2}_{-3.2}$	–	–	$^{+1.5}_{-1.8}$	±3.6	±0.3	$^{+1.5}_{-1.5}$
110 - 127	$^{+16.2}_{-14.4}$	$^{+3.7}_{-3.5}$	–	–	$^{+1.6}_{-1.9}$	±3.7	±0.2	$^{+1.4}_{-1.4}$
127 - 146	$^{+19.2}_{-16.9}$	$^{+4.3}_{-4.0}$	–	–	$^{+1.8}_{-2.0}$	±3.7	±0.1	$^{+1.4}_{-1.4}$
146 - 169	$^{+22.8}_{-19.8}$	$^{+5.0}_{-4.6}$	–	–	$^{+2.1}_{-2.1}$	±3.8	±0.2	$^{+1.4}_{-1.3}$
169 - 195	$^{+27.7}_{-23.0}$	$^{+6.0}_{-5.4}$	$^{+1.3}_{-0.9}$	–	$^{+2.5}_{-2.3}$	±3.8	±0.5	$^{+1.4}_{-1.3}$
195 - 224	$^{+34.9}_{-26.7}$	$^{+7.0}_{-6.4}$	$^{+5.3}_{-5.6}$	–	$^{+3.0}_{-2.7}$	±3.8	±1.1	$^{+1.4}_{-1.3}$
224 - 259	$^{+46.0}_{-32.4}$	$^{+8.1}_{-8.0}$	$^{+11.0}_{-11.1}$	–	$^{+3.5}_{-3.3}$	±3.8	±2.1	$^{+1.4}_{-1.3}$
259 - 298	$^{+52.9}_{-44.5}$	$^{+9.1}_{-10.5}$	$^{+19.1}_{-17.5}$	–	$^{+3.9}_{-4.4}$	±3.8	±3.7	$^{+1.4}_{-1.3}$

TABLE III: Systematic uncertainties (in percent) on the measured inclusive jet differential cross section as a function of $p_{\rm T}^{\rm jet}$ for jets in the regions $0.7 < |y^{\rm jet}| < 1.1$, $1.1 < |y^{\rm jet}| < 1.6$, and $1.6 < |y^{\rm jet}| < 2.1$ (see Fig. 7). The different columns follow the discussion in Section X. An additional 5.8% uncertainty on the integrated luminosity is not included.

$\frac{d^2\sigma}{dp_{\rm T}^{\rm jet}dy^{\rm jet}}$ $(\lvert y^{\rm jet}\rvert < 0.1)$		
$p_{\rm T}^{\rm jet}$ [GeV/c]	$\sigma \pm (stat.) \pm (sys.)$ [nb/(GeV/c)]	$C_{\rm HAD}$ parton $\rightarrow$ hadron
54 - 62	$(14.5 \pm 0.5^{+2.0}_{-1.9}) \times 10^{0}$	1.177 ± 0.124
62 - 72	$(6.68 \pm 0.08^{+0.85}_{-0.84}) \times 10^{0}$	1.144 ± 0.097
72 - 83	$(2.87 \pm 0.05^{+0.35}_{-0.34}) \times 10^{0}$	1.119 ± 0.077
83 - 96	$(1.24 \pm 0.02^{+0.14}_{-0.14}) \times 10^{0}$	1.098 ± 0.061
96 - 110	$(5.31 \pm 0.11^{+0.60}_{-0.61}) \times 10^{-1}$	1.083 ± 0.049
110 - 127	$(2.33 \pm 0.06^{+0.27}_{-0.26}) \times 10^{-1}$	1.070 ± 0.039
127 - 146	$(9.36 \pm 0.12^{+1.10}_{-1.08}) \times 10^{-2}$	1.060 ± 0.032
146 - 169	$(3.63 \pm 0.06^{+0.45}_{-0.43}) \times 10^{-2}$	1.052 ± 0.026
169 - 195	$(1.39 \pm 0.01^{+0.19}_{-0.18}) \times 10^{-2}$	1.046 ± 0.021
195 - 224	$(5.22 \pm 0.06^{+0.77}_{-0.72}) \times 10^{-3}$	1.041 ± 0.017
224 - 259	$(1.79 \pm 0.03^{+0.29}_{-0.27}) \times 10^{-3}$	1.037 ± 0.013
259 - 298	$(5.92 \pm 0.11^{+1.08}_{-1.00}) \times 10^{-4}$	1.034 ± 0.010
298 - 344	$(1.78 \pm 0.06^{+0.36}_{-0.33}) \times 10^{-4}$	1.032 ± 0.007
344 - 396	$(4.68 \pm 0.28^{+1.08}_{-0.94}) \times 10^{-5}$	1.030 ± 0.005
396 - 457	$(1.29 \pm 0.12^{+0.34}_{-0.29}) \times 10^{-5}$	1.028 ± 0.002
457 - 527	$(2.47 \pm 0.50^{+0.80}_{-0.68}) \times 10^{-6}$	1.027 ± 0.001
527 - 700	$(2.13 \pm 0.95^{+0.97}_{-0.75}) \times 10^{-7}$	1.026 ± 0.006
$\frac{d^2\sigma}{dp_{\rm T}^{\rm jet}dy^{\rm jet}}$ $(0.1 < \lvert y^{\rm jet}\rvert < 0.7)$		
$p_{\rm T}^{\rm jet}$ [GeV/c]	$\sigma \pm (stat.) \pm (sys.)$ [nb/(GeV/c)]	$C_{\rm HAD}$ parton $\rightarrow$ hadron
54 - 62	$(14.0 \pm 0.20^{+1.6}_{-1.6}) \times 10^{0}$	1.188 ± 0.140
62 - 72	$(6.14 \pm 0.12^{+0.66}_{-0.65}) \times 10^{0}$	1.156 ± 0.113
72 - 83	$(2.69 \pm 0.02^{+0.29}_{-0.27}) \times 10^{0}$	1.129 ± 0.091
83 - 96	$(1.14 \pm 0.01^{+0.12}_{-0.11}) \times 10^{0}$	1.108 ± 0.073
96 - 110	$(4.90 \pm 0.04^{+0.51}_{-0.48}) \times 10^{-1}$	1.090 ± 0.059
110 - 127	$(2.08 \pm 0.02^{+0.22}_{-0.21}) \times 10^{-1}$	1.076 ± 0.047
127 - 146	$(8.51 \pm 0.04^{+0.95}_{-0.89}) \times 10^{-2}$	1.065 ± 0.038
146 - 169	$(3.33 \pm 0.02^{+0.40}_{-0.37}) \times 10^{-2}$	1.055 ± 0.029
169 - 195	$(1.23 \pm 0.01^{+0.16}_{-0.15}) \times 10^{-2}$	1.047 ± 0.023
195 - 224	$(4.53 \pm 0.02^{+0.65}_{-0.61}) \times 10^{-3}$	1.041 ± 0.017
224 - 259	$(1.57 \pm 0.01^{+0.26}_{-0.24}) \times 10^{-3}$	1.036 ± 0.012
259 - 298	$(4.87 \pm 0.06^{+0.91}_{-0.83}) \times 10^{-4}$	1.031 ± 0.007
298 - 344	$(1.43 \pm 0.02^{+0.31}_{-0.27}) \times 10^{-4}$	1.028 ± 0.003
344 - 396	$(3.69 \pm 0.10^{+0.94}_{-0.80}) \times 10^{-5}$	1.025 ± 0.001
396 - 457	$(7.18 \pm 0.34^{+2.20}_{-1.80}) \times 10^{-6}$	1.023 ± 0.004
457 - 527	$(1.16 \pm 0.13^{+0.44}_{-0.35}) \times 10^{-6}$	1.021 ± 0.008
527 - 700	$(8.97 \pm 2.40^{+4.75}_{-3.64}) \times 10^{-8}$	1.018 ± 0.014

TABLE IV: Measured inclusive jet differential cross section as a function of $p_{\rm T}^{\rm jet}$ for jets in the regions $|y^{\rm jet}| < 0.1$ and $0.1 < |y^{\rm jet}| < 0.7$ (see Fig. 9). An additional 5.8% uncertainty on the integrated luminosity is not included. The parton-to-hadron correction factors, $C_{\rm HAD}(p_{\rm T}^{\rm jet}, y^{\rm jet})$, are applied to the pQCD predictions (see Fig. 8).

$\frac{d^2\sigma}{dp_{\rm T}^{\rm jet}dy^{\rm jet}}$ $(0.7 < \lvert y^{\rm jet}\rvert < 1.1)$		
$p_{\rm T}^{\rm jet}$ [GeV/c]	$\sigma \pm (stat.) \pm (sys.)$ [nb/(GeV/c)]	$C_{\rm HAD}$ parton $\rightarrow$ hadron
54 - 62	$(12.3 \pm 0.2^{+1.5}_{-1.5}) \times 10^{0}$	1.169 ± 0.125
62 - 72	$(5.48 \pm 0.14^{+0.65}_{-0.65}) \times 10^{0}$	1.143 ± 0.103
72 - 83	$(2.40 \pm 0.02^{+0.28}_{-0.27}) \times 10^{0}$	1.120 ± 0.085
83 - 96	$(1.00 \pm 0.01^{+0.15}_{-0.11}) \times 10^{0}$	1.102 ± 0.070
96 - 110	$(4.15 \pm 0.05^{+0.48}_{-0.46}) \times 10^{-1}$	1.087 ± 0.057
110 - 127	$(1.73 \pm 0.03^{+0.21}_{-0.20}) \times 10^{-1}$	1.075 ± 0.047
127 - 146	$(6.83 \pm 0.05^{+0.87}_{-0.82}) \times 10^{-2}$	1.064 ± 0.038
146 - 169	$(2.52 \pm 0.03^{+0.35}_{-0.33}) \times 10^{-2}$	1.056 ± 0.031
169 - 195	$(8.95 \pm 0.06^{+1.36}_{-1.26}) \times 10^{-3}$	1.048 ± 0.024
195 - 224	$(3.04 \pm 0.02^{+0.51}_{-0.47}) \times 10^{-3}$	1.042 ± 0.019
224 - 259	$(9.52 \pm 0.11^{+1.82}_{-1.68}) \times 10^{-4}$	1.037 ± 0.014
259 - 298	$(2.53 \pm 0.05^{+0.56}_{-0.51}) \times 10^{-4}$	1.033 ± 0.009
298 - 344	$(6.18 \pm 0.17^{+1.64}_{-1.49}) \times 10^{-5}$	1.030 ± 0.005
344 - 396	$(1.11 \pm 0.07^{+0.36}_{-0.31}) \times 10^{-5}$	1.027 ± 0.001
396 - 457	$(1.53 \pm 0.20^{+0.65}_{-0.50}) \times 10^{-6}$	1.025 ± 0.003
457 - 527	$(2.17 \pm 0.72^{+1.25}_{-0.88}) \times 10^{-7}$	1.023 ± 0.007
$\frac{d^2\sigma}{dp_{\rm T}^{\rm jet}dy^{\rm jet}}$ $(1.1 < \lvert y^{\rm jet}\rvert < 1.6)$		
$p_{\rm T}^{\rm jet}$ [GeV/c]	$\sigma \pm (stat.) \pm (sys.)$ [nb/(GeV/c)]	$C_{\rm HAD}$ parton $\rightarrow$ hadron
54 - 62	$(11.0 \pm 0.3^{+1.4}_{-1.3}) \times 10^{0}$	1.160 ± 0.125
62 - 72	$(4.40 \pm 0.15^{+0.54}_{-0.53}) \times 10^{0}$	1.133 ± 0.101
72 - 83	$(1.82 \pm 0.06^{+0.22}_{-0.22}) \times 10^{0}$	1.111 ± 0.081
83 - 96	$(7.22 \pm 0.37^{+0.90}_{-0.90}) \times 10^{-1}$	1.094 ± 0.065
96 - 110	$(2.98 \pm 0.05^{+0.38}_{-0.38}) \times 10^{-1}$	1.080 ± 0.052
110 - 127	$(1.14 \pm 0.03^{+0.15}_{-0.15}) \times 10^{-1}$	1.068 ± 0.042
127 - 146	$(4.10 \pm 0.04^{+0.60}_{-0.60}) \times 10^{-2}$	1.059 ± 0.034
146 - 169	$(1.39 \pm 0.02^{+0.22}_{-0.23}) \times 10^{-2}$	1.051 ± 0.027
169 - 195	$(4.19 \pm 0.04^{+0.78}_{-0.76}) \times 10^{-3}$	1.045 ± 0.021
195 - 224	$(1.15 \pm 0.02^{+0.25}_{-0.24}) \times 10^{-3}$	1.040 ± 0.016
224 - 259	$(2.73 \pm 0.09^{+0.73}_{-0.64}) \times 10^{-4}$	1.036 ± 0.012
259 - 298	$(5.18 \pm 0.23^{+1.68}_{-1.39}) \times 10^{-5}$	1.033 ± 0.009
298 - 344	$(7.99 \pm 0.61^{+3.31}_{-2.56}) \times 10^{-6}$	1.030 ± 0.006
344 - 396	$(1.05 \pm 0.22^{+0.71}_{-0.45}) \times 10^{-6}$	1.028 ± 0.003
$\frac{d^2\sigma}{dp_{\rm T}^{\rm jet}dy^{\rm jet}}$ $(1.6 < \lvert y^{\rm jet}\rvert < 2.1)$		
$p_{\rm T}^{\rm jet}$ [GeV/c]	$\sigma \pm (stat.) \pm (sys.)$ [nb/(GeV/c)]	$C_{\rm HAD}$ parton $\rightarrow$ hadron
54 - 62	$(6.67 \pm 0.15^{+0.84}_{-0.75}) \times 10^{0}$	1.132 ± 0.104
62 - 72	$(2.68 \pm 0.02^{+0.32}_{-0.30}) \times 10^{0}$	1.116 ± 0.087
72 - 83	$(1.04 \pm 0.01^{+0.12}_{-0.12}) \times 10^{0}$	1.100 ± 0.072
83 - 96	$(3.77 \pm 0.04^{+0.49}_{-0.46}) \times 10^{-1}$	1.086 ± 0.058
96 - 110	$(1.32 \pm 0.02^{+0.19}_{-0.18}) \times 10^{-1}$	1.072 ± 0.045
110 - 127	$(4.18 \pm 0.04^{+0.72}_{-0.65}) \times 10^{-2}$	1.059 ± 0.033
127 - 146	$(1.21 \pm 0.02^{+0.24}_{-0.22}) \times 10^{-2}$	1.047 ± 0.022
146 - 169	$(2.92 \pm 0.04^{+0.70}_{-0.61}) \times 10^{-3}$	1.035 ± 0.012
169 - 195	$(5.74 \pm 0.09^{+1.65}_{-1.38}) \times 10^{-4}$	1.024 ± 0.003
195 - 224	$(8.49 \pm 0.31^{+3.09}_{-2.42}) \times 10^{-5}$	1.013 ± 0.005
224 - 259	$(8.65 \pm 0.63^{+4.18}_{-3.08}) \times 10^{-6}$	1.003 ± 0.012
259 - 298	$(5.67 \pm 1.65^{+3.25}_{-2.80}) \times 10^{-7}$	0.993 ± 0.018

TABLE V: Measured inclusive jet differential cross section as a function of $p_{\rm T}^{\rm jet}$ for jets in the regions $0.7 < |y^{\rm jet}| < 1.1$, $1.1 < |y^{\rm jet}| < 1.6$, and $1.6 < |y^{\rm jet}| < 2.1$ (see Fig. 9). An additional 5.8% uncertainty on the integrated luminosity is not included. The parton-to-hadron correction factors, $C_{\rm HAD}(p_{\rm T}^{\rm jet}, y^{\rm jet})$, are applied to the pQCD predictions (see Fig. 8).

Systematic uncertainties [%] $(0.1 < \lvert y^{\rm jet}\rvert < 0.7)$ $(D = 0.5)$					
$p_{\rm T}^{\rm jet}$ [GeV/c]	jet energy scale	resolution	unfolding	$p_{\rm T}^{\rm jet}$-spectra	$\delta_{p_{\rm T}}^{\rm mi}$
54 - 62	$^{+9.9}_{-9.2}$	$^{+2.4}_{-2.3}$	±5.4	±0.6	$^{+0.8}_{-0.8}$
62 - 72	$^{+9.8}_{-9.0}$	$^{+2.4}_{-2.2}$	±4.8	±0.6	$^{+0.7}_{-0.7}$
72 - 83	$^{+9.8}_{-8.9}$	$^{+2.3}_{-2.2}$	±4.3	±0.6	$^{+0.6}_{-0.7}$
83 - 96	$^{+9.7}_{-8.9}$	$^{+2.2}_{-2.1}$	±3.8	±0.6	$^{+0.6}_{-0.6}$
96 - 110	$^{+9.8}_{-9.0}$	$^{+2.2}_{-2.1}$	±3.4	±0.6	$^{+0.5}_{-0.5}$
110 - 127	$^{+10.0}_{-9.4}$	$^{+2.1}_{-2.0}$	±3.1	±0.6	$^{+0.5}_{-0.5}$
127 - 146	$^{+10.4}_{-9.9}$	$^{+2.1}_{-2.0}$	±2.8	±0.6	$^{+0.4}_{-0.4}$
146 - 169	$^{+11.2}_{-10.8}$	$^{+2.1}_{-2.0}$	±2.5	±0.5	$^{+0.4}_{-0.4}$
169 - 195	$^{+12.5}_{-11.9}$	$^{+2.1}_{-2.1}$	±2.3	±0.4	$^{+0.4}_{-0.4}$
195 - 224	$^{+14.3}_{-13.3}$	$^{+2.2}_{-2.2}$	±2.1	±0.3	$^{+0.4}_{-0.3}$
224 - 259	$^{+16.6}_{-15.0}$	$^{+2.4}_{-2.4}$	±1.9	±0.2	$^{+0.3}_{-0.3}$
259 - 298	$^{+19.3}_{-17.0}$	$^{+2.7}_{-2.7}$	±1.8	±0.1	$^{+0.3}_{-0.3}$
298 - 344	$^{+22.3}_{-19.4}$	$^{+3.1}_{-3.2}$	±1.6	±0.1	$^{+0.3}_{-0.3}$
344 - 396	$^{+25.7}_{-22.1}$	$^{+3.7}_{-3.8}$	±1.5	±0.2	$^{+0.3}_{-0.3}$
396 - 457	$^{+30.7}_{-25.5}$	$^{+4.5}_{-4.6}$	±1.4	±0.5	$^{+0.3}_{-0.3}$
457 - 527	$^{+39.5}_{-29.7}$	$^{+5.5}_{-5.6}$	±1.3	±1.3	$^{+0.3}_{-0.2}$
527 - 700	$^{+52.6}_{-37.7}$	$^{+7.4}_{-7.3}$	±1.2	±4.2	$^{+0.3}_{-0.2}$

Systematic uncertainties [%] $(0.1 < \lvert y^{\rm jet}\rvert < 0.7)$ $(D = 1.0)$					
$p_{\rm T}^{\rm jet}$ [GeV/c]	jet energy scale	resolution	unfolding	$p_{\rm T}^{\rm jet}$-spectra	$\delta_{p_{\rm T}}^{\rm mi}$
54 - 62	$^{+10.7}_{-9.4}$	$^{+2.7}_{-2.7}$	±5.6	±0.4	$^{+3.5}_{-2.9}$
62 - 72	$^{+10.4}_{-9.3}$	$^{+2.6}_{-2.5}$	±4.9	±0.4	$^{+3.0}_{-2.6}$
72 - 83	$^{+10.3}_{-9.2}$	$^{+2.4}_{-2.4}$	±4.2	±0.4	$^{+2.6}_{-2.4}$
83 - 96	$^{+10.2}_{-9.2}$	$^{+2.3}_{-2.3}$	±3.7	±0.4	$^{+2.3}_{-2.2}$
96 - 110	$^{+10.2}_{-9.3}$	$^{+2.2}_{-2.2}$	±3.2	±0.4	$^{+2.1}_{-2.0}$
110 - 127	$^{+10.4}_{-9.6}$	$^{+2.1}_{-2.1}$	±2.8	±0.4	$^{+1.9}_{-1.8}$
127 - 146	$^{+10.8}_{-10.1}$	$^{+2.0}_{-2.0}$	±2.5	±0.4	$^{+1.7}_{-1.7}$
146 - 169	$^{+11.5}_{-10.8}$	$^{+1.9}_{-1.9}$	±2.1	±0.4	$^{+1.6}_{-1.6}$
169 - 195	$^{+12.6}_{-11.8}$	$^{+1.9}_{-2.0}$	±1.9	±0.4	$^{+1.5}_{-1.4}$
195 - 224	$^{+13.9}_{-13.1}$	$^{+1.9}_{-2.0}$	±1.6	±0.3	$^{+1.4}_{-1.3}$
224 - 259	$^{+15.8}_{-14.7}$	$^{+2.1}_{-2.2}$	±1.4	±0.3	$^{+1.3}_{-1.3}$
259 - 298	$^{+18.0}_{-16.6}$	$^{+2.4}_{-2.5}$	±1.3	±0.2	$^{+1.3}_{-1.2}$
298 - 344	$^{+20.8}_{-18.8}$	$^{+2.8}_{-2.9}$	±1.1	±0.2	$^{+1.2}_{-1.1}$
344 - 396	$^{+24.5}_{-21.4}$	$^{+3.4}_{-3.6}$	±1.0	±0.2	$^{+1.2}_{-1.1}$
396 - 457	$^{+30.1}_{-24.7}$	$^{+4.3}_{-4.4}$	±0.8	±0.5	$^{+1.1}_{-1.0}$
457 - 527	$^{+38.8}_{-29.5}$	$^{+5.4}_{-5.4}$	±0.7	±1.1	$^{+1.1}_{-1.0}$
527 - 700	$^{+49.8}_{-37.6}$	$^{+7.3}_{-7.2}$	±0.6	±3.4	$^{+1.0}_{-0.9}$

TABLE VI: Systematic uncertainties (in percent) on the measured inclusive jet differential cross section as a function of $p_{\rm T}^{\rm jet}$, for jets in the region $0.1 < |y^{\rm jet}| < 0.7$ and using $D = 0.5$ and $D = 1.0$ (see Fig. 11). The different columns follow the discussion in Section X. An additional 5.8% uncertainty on the integrated luminosity is not included.

$\frac{d^2\sigma}{dp_{\rm T}^{\rm jet}dy^{\rm jet}}$ $(0.1 < \lvert y^{\rm jet}\rvert < 0.7)$ $(D = 0.5)$		
$p_{\rm T}^{\rm jet}$ [GeV/c]	$\sigma \pm (stat.) \pm (sys.)$ [nb/(GeV/c)]	$C_{\rm HAD}$ parton $\rightarrow$ hadron
54 - 62	$(10.5 \pm 0.2^{+1.2}_{-1.1}) \times 10^{0}$	1.089 ± 0.104
62 - 72	$(4.81 \pm 0.03^{+0.54}_{-0.50}) \times 10^{0}$	1.076 ± 0.086
72 - 83	$(2.09 \pm 0.01^{+0.23}_{-0.21}) \times 10^{0}$	1.064 ± 0.070
83 - 96	$(0.91 \pm 0.01^{+0.10}_{-0.09}) \times 10^{0}$	1.055 ± 0.057
96 - 110	$(3.95 \pm 0.04^{+0.42}_{-0.39}) \times 10^{-1}$	1.047 ± 0.047
110 - 127	$(1.71 \pm 0.02^{+0.18}_{-0.17}) \times 10^{-1}$	1.041 ± 0.037
127 - 146	$(0.71 \pm 0.01^{+0.08}_{-0.07}) \times 10^{-1}$	1.035 ± 0.029
146 - 169	$(2.76 \pm 0.02^{+0.32}_{-0.31}) \times 10^{-2}$	1.030 ± 0.023
169 - 195	$(1.04 \pm 0.01^{+0.14}_{-0.13}) \times 10^{-2}$	1.026 ± 0.017
195 - 224	$(3.87 \pm 0.02^{+0.57}_{-0.53}) \times 10^{-3}$	1.022 ± 0.012
224 - 259	$(1.34 \pm 0.01^{+0.23}_{-0.21}) \times 10^{-3}$	1.019 ± 0.008
259 - 298	$(4.26 \pm 0.04^{+0.83}_{-0.74}) \times 10^{-4}$	1.017 ± 0.005
298 - 344	$(1.22 \pm 0.02^{+0.28}_{-0.24}) \times 10^{-4}$	1.015 ± 0.002
344 - 396	$(3.16 \pm 0.09^{+0.82}_{-0.71}) \times 10^{-5}$	1.013 ± 0.001
396 - 457	$(6.30 \pm 0.32^{+1.96}_{-1.63}) \times 10^{-6}$	1.011 ± 0.002
457 - 527	$(1.01 \pm 0.12^{+0.40}_{-0.31}) \times 10^{-6}$	1.010 ± 0.003
527 - 700	$(0.83 \pm 0.23^{+0.44}_{-0.32}) \times 10^{-7}$	1.008 ± 0.005
$\frac{d^2\sigma}{dp_{\rm T}^{\rm jet}dy^{\rm jet}}$ $(0.1 < \lvert y^{\rm jet}\rvert < 0.7)$ $(D = 1.0)$		
$p_{\rm T}^{\rm jet}$ [GeV/c]	$\sigma \pm (stat.) \pm (sys.)$ [nb/(GeV/c)]	$C_{\rm HAD}$ parton $\rightarrow$ hadron
54 - 62	$(20.0 \pm 0.2^{+2.6}_{-2.3}) \times 10^{0}$	1.372 ± 0.227
62 - 72	$(8.65 \pm 0.04^{+1.1}_{-1.0}) \times 10^{0}$	1.296 ± 0.171
72 - 83	$(3.59 \pm 0.02^{+0.42}_{-0.39}) \times 10^{0}$	1.236 ± 0.129
83 - 96	$(1.49 \pm 0.01^{+0.17}_{-0.16}) \times 10^{0}$	1.190 ± 0.098
96 - 110	$(6.27 \pm 0.05^{+0.70}_{-0.65}) \times 10^{-1}$	1.155 ± 0.075
110 - 127	$(2.63 \pm 0.03^{+0.29}_{-0.27}) \times 10^{-1}$	1.127 ± 0.057
127 - 146	$(1.05 \pm 0.01^{+0.12}_{-0.11}) \times 10^{-1}$	1.105 ± 0.044
146 - 169	$(4.04 \pm 0.03^{+0.48}_{-0.45}) \times 10^{-2}$	1.088 ± 0.034
169 - 195	$(1.48 \pm 0.01^{+0.19}_{-0.18}) \times 10^{-2}$	1.075 ± 0.026
195 - 224	$(5.41 \pm 0.02^{+0.77}_{-0.73}) \times 10^{-3}$	1.065 ± 0.019
224 - 259	$(1.86 \pm 0.01^{+0.30}_{-0.28}) \times 10^{-3}$	1.057 ± 0.013
259 - 298	$(5.77 \pm 0.04^{+1.05}_{-1.00}) \times 10^{-4}$	1.050 ± 0.008
298 - 344	$(1.70 \pm 0.02^{+0.36}_{-0.32}) \times 10^{-4}$	1.045 ± 0.003
344 - 396	$(4.26 \pm 0.10^{+1.05}_{-0.93}) \times 10^{-5}$	1.041 ± 0.003
396 - 457	$(8.17 \pm 0.36^{+2.49}_{-2.06}) \times 10^{-6}$	1.038 ± 0.009
457 - 527	$(1.39 \pm 0.14^{+0.55}_{-0.42}) \times 10^{-6}$	1.036 ± 0.015
527 - 700	$(1.19 \pm 0.27^{+0.60}_{-0.46}) \times 10^{-7}$	1.033 ± 0.027

TABLE VII: Measured inclusive jet differential cross section as a function of $p_{\rm T}^{\rm jet}$ for jets in the region $0.1 < |y^{\rm jet}| < 0.7$ using $D = 0.5$ and $D = 1.0$ (see Fig. 11). An additional 5.8% uncertainty on the integrated luminosity is not included. The parton-to-hadron correction factors, $C_{\rm HAD}(p_{\rm T}^{\rm jet})$, are applied to the pQCD predictions.

APPENDIX A: CORRELATIONS OF SYSTEMATIC UNCERTAINTIES

The correlations among systematic uncertainties in different $p_{\rm T}^{\rm jet}$ bins and $|y^{\rm jet}|$ regions are studied in detail. The uncertainty on the absolute jet energy scale is decomposed into different sources considered independent but fully correlated across $p_{\rm T}^{\rm jet}$ bins and $|y^{\rm jet}|$ regions. A $\pm 1.8\%$ uncertainty on the absolute energy scale, independent of $p_{\rm T}^{\rm jet}$, results from the sum in quadrature of four different contributions [42]: a $\pm 0.5\%$ uncertainty from the calorimeter stability versus time, a $\pm 1.0\%$ uncertainty due to the modeling of the jet fragmentation, a $\pm 0.5\%$ uncertainty from the simulation of the electromagnetic calorimeter response, and a $\pm 1.3\%$ uncertainty from the simulation of the calorimeter response at the boundary between calorimeter towers. Other contributions to the absolute energy scale uncertainty come from the description of the calorimeter response to hadrons for different ranges in hadron momentum [42]. Table VIII shows the resulting relative contributions to the quoted systematic uncertainty on the measured cross sections related to the absolute jet energy scale uncertainty.

$p_{\rm T}^{\rm jet}$	$p_{\rm T}^{\rm jet}$ independent	response to hadrons		
[GeV/c]	uncertainty	$p < 12$ GeV/c	$12 < p < 20$ GeV/c	$p > 20$ GeV/c
54 - 62	90.3	37.8	15.2	13.5
62 - 72	90.2	35.2	16.1	19.1
72 - 83	89.9	31.9	17.0	24.6
83 - 96	89.2	28.8	17.3	30.1
96 - 110	88.0	26.0	16.9	35.8
110 - 127	86.4	22.7	16.4	41.9
127 - 146	84.3	20.0	15.1	47.7
146 - 169	82.1	17.2	14.1	52.6
169 - 195	79.8	14.6	12.7	57.0
195 - 224	77.6	12.5	11.5	60.7
224 - 259	75.7	10.7	10.3	63.6
259 - 298	73.8	9.1	9.2	66.2
298 - 344	72.1	7.8	8.2	68.3
344 - 396	70.5	6.8	7.3	70.2
396 - 457	69.2	5.8	6.4	71.7
457 - 527	68.0	5.0	5.7	72.9
527 - 700	66.8	4.2	5.0	74.2

TABLE VIII: Relative contributions (in percent) to the quoted systematic uncertainty on the measured cross sections related to the absolute jet energy scale uncertainty. The second column corresponds to a $\pm 1.8\%$ uncertainty on the absolute energy scale, as discussed in the text. Sources are considered independent and fully correlated in $p_{\rm T}^{\rm jet}$ and $|y^{\rm jet}|$.

The rest of the systematic uncertainties on the measured cross sections, including that on the total integrated luminosity, are also assumed to be independent and fully correlated across $p_{\rm T}^{\rm jet}$ bins and $|y^{\rm jet}|$ regions, except those related to the $\beta_{\rm data}/\beta_{\rm mc}$ ratio, for which uncertainties in different $|y^{\rm jet}|$ regions are uncorrelated.

A global χ^2 test is performed according to the formula

$$\chi^2 = \sum_{j=1}^{76} \frac{[\sigma_j^d - \sigma_j^{th}(\bar{s})]^2}{[\delta\sigma_j^d]^2 + [\delta\sigma_j^{th}(\bar{s})]^2} + \sum_{i=1}^{17} [s_i]^2 \ , \tag{A1}$$

where σ_j^d is the measured cross section for data point j, $\sigma_j^{th}(\bar{s})$ is the corresponding prediction, and $\bar{s}$ denotes the vector of standard deviations, s_i, for the different independent sources of systematic uncertainty. The values for $\sigma_j^{th}(\bar{s})$ are obtained from the nominal NLO pQCD prediction, where $\bar{s}$ includes the uncertainty on $C_{\rm HAD}$ but does not consider PDF uncertainties. The uncertainty on $C_{\rm HAD}$ is assumed to be fully correlated across $p_{\rm T}^{\rm jet}$ bins and $|y^{\rm jet}|$ regions. The sums in Eq. (A1) run over 76 data points and 17 independent sources of systematic uncertainty, and the χ^2 is minimized with respect to $\bar{s}$. Correlations among systematic uncertainties are taken into account in $\sigma_j^{th}(\bar{s})$. As an example, for a given source i, variations of s_i will coherently affect all the $\sigma_j^{th}(\bar{s})$ values if the corresponding systematic uncertainties are considered fully correlated across $p_{\rm T}^{\rm jet}$ bins and $|y^{\rm jet}|$ regions.